© 2021. This manuscript version is made available under the CC-BY-NC-ND 4.0 license http://creativecommons.org/licenses/by-nc-nd/4.0/

# Role of ocean tidal asymmetry and estuarine geometry in the fate of plastic debris from ocean sources within tidal estuaries

Paula Núñez[a,*], Sonia Castanedo[b], Raúl Medina[a]

[a]*IHCantabria - Instituto de Hidráulica Ambiental de la Universidad de Cantabria*
[b]*Departamento de Ciencias y Técnicas del Agua y del Medio Ambiente, E.T.S.I. de Caminos, Canales y Puertos, Universidad de Cantabria, Avda. de los Castros s/n, Santander, Spain*

## Abstract

Tidal asymmetry drives the transport of materials (e.g. plastic debris) within tidal estuaries. Most previous research has focused on the asymmetry that arises within estuaries and relates to sediment transport; however, estuaries exhibiting tidal asymmetry at the mouth and their relationship with materials other than sediments have received less attention. This study uses numerical hydrodynamic and Lagrangian transport models to assess the effect of estuary morphology on the propagation of asymmetric tides and how it influences the distribution of plastic debris that reaches tidal estuaries from ocean sources. A series of numerical experiments were conducted in idealised estuaries, specifically in tidal creeks. The results show that the asymmetry at the mouth results in flood/ebb dominance and influences the presence of plastic debris in areas where the main channel favours tidal flow. Flood-dominated estuaries show an import capacity 50% higher than those that show symmetric or negative asymmetric tides at their mouths. Numerical simulations show that the relevant role in defining flood or ebb

*Corresponding author

© 2021. This manuscript version is made available under the CC-BY-NC-ND 4.0 license http://creativecommons.org/licenses/by-nc-nd/4.0/

dominance is played by the geometry of the estuary when increased friction that opposes flow and intertidal storage areas are present, although small influences of the external tidal asymmetry are also appreciated. The probability of plastic debris presence was 90% for positive asymmetric tides and varied between and 70-80% for symmetric and negative-asymmetric tides. A remarkable finding of this study is the regulatory role of kurtosis which corrects the tendency induced by skewness in the fate of plastic debris. These findings were corroborated with the application of this methodology to a real estuary and a comparison of the obtained results with available field data on plastic debris.

*Keywords:*
Tidal asymmetry, Estuary, Numerical model, Plastic debris, Lagrangian transport model

## 1. Introduction

Marine litter is one of the main threats to marine environments, causing significant ecological, economic, and social damages (UNEP, 2005). Currently, marine litter has become a priority issue in international environmental agendas, such as the EU Marine Strategy Framework Directive (MSFD) (Galgani et al., 2013). Approximately 80% of marine litter is made of plastics (Barnes et al., 2009; Derraik, 2002). In 2010, between 4.8 and 12.7 million tons of plastic debris accumulated in the ocean, and an increase of an order of magnitude has been estimated for 2025 (Jambeck et al., 2015). Approximately 80% of the litter that reaches marine environments comes from land-based sources, mainly rivers (Galgani et al., 2015; Rech et al., 2014). A significant part of this litter will reach the open ocean, and the remaining litter will be retained within estuarine systems, which often act

© 2021. This manuscript version is made available under the CC-BY-NC-ND 4.0 license http://creativecommons.org/licenses/by-nc-nd/4.0/

as marine litter sinks with a notable plastic fraction (Acha et al., 2003). Furthermore, tides and waves can also interact to introduce litter from sea-based sources (e.g. trawling) into estuarine environments (Hinojosa and Thiel, 2009).

Estuaries are transition areas that are subject to marine events, such as tide, waves, and the influx of saline water, and riverine influences, such as river and sediment discharge. These areas show high biological productivity and provide habitats for many species of flora and fauna. Countless species of fish, crustaceans, and shellfish depend on estuarine waters as safe places for their survival. In addition, estuaries serve as refuges for a wide variety of aquatic birds, whether autochthonous or exotic. Moreover, they have a key role in coastal protection and carbon capture, as well as the socioeconomic importance of estuaries for the development of different local activities such as fishing, shellfishing, small industry, tourism, and recreational activities (Barbier et al., 2011). Therefore, the accumulation of marine litter in general and plastic debris in particular represents a significant threat to estuarine habitats and the ecosystem services they provide (Mazarrasa et al., 2019).

Consequently, there is growing concern regarding the issue of marine litter, especially plastic debris, at the estuarine scale by defining prevention and clean-up strategies. The study of plastic debris hotspots, areas of greatest concentration, allows us to focus clean-up efforts on priority areas and thus reduce the associated costs (Gallo et al., 2018; Hall, 2000; OSPAR, 2009). The availability of this type of information on an estuarine scale is limited, which makes the organisation and logistics of these activities difficult for managers. Most existing studies that assess the transport and fate of litter only conduct global analyses and identify large concentrations in areas of oceanic convergence (gyres) (Law et al., 2010; Lebreton et al., 2012;

© 2021. This manuscript version is made available under the CC-BY-NC-ND 4.0 license http://creativecommons.org/licenses/by-nc-nd/4.0/

Maximenko et al., 2012; Van Sebille et al., 2012), while regional studies have been performed in confined areas, such as the East Asian seas (Isobe et al., 2009; Kako et al., 2014, 2011; Yoon et al., 2010), the waters near the Hawaiian Islands (Carson et al., 2013; Kubota, 1994), or the Mediterranean Sea (Zambianchi et al., 2017, 2014). Nevertheless, studies focusing on an estuary scale are much rarer, and most are based on field observations in specific estuaries, making it difficult to draw general conclusions (Browne et al., 2010; Klein et al., 2015; Mazarrasa et al., 2019; Yonkos et al., 2014).

Some research, such as that of Ballent et al. (2012); Browne et al. (2010); Costa et al. (2011); Eerkes-Medrano et al. (2015); Galgani et al. (2000), suggest that the study of plastic debris transport within estuaries can be assimilated to the study of sediment transport. Most published theories and studies relate sediment transport mechanisms and morphological trends in estuaries with the *tidal asymmetry* that arises with tidal propagation through these environments. Aubrey and Speer (1985); Dronkers (1986); Friedrichs and Aubrey (1988), and Speer and Aubrey (1985) analysed the propagation of symmetric tides through estuaries with different geometries using analytical models or field observations to draw a series of relevant conclusions. Tidal wave deforms as it propagates through shallow estuaries owing to the friction related to the lateral boundaries and the bottom. This deformation results in differences between flood- and ebb-phase durations and, consequently, the intensities of the flood and ebb currents. Therefore, tidal asymmetry induces net transport in the direction of the most intense currents, which determines the estuarine trends that import or export sediments. If the flood phase is shorter, the tidal asymmetry is considered positive, and the flood currents are faster than the ebb currents, and vice versa for a negative tidal asymmetry. Regarding estuarine geometries, estuaries

© 2021. This manuscript version is made available under the CC-BY-NC-ND 4.0 license http://creativecommons.org/licenses/by-nc-nd/4.0/

where tidal flats occupy a small area or show high friction typically develop positive asymmetry and a tendency to import sediments. In contrast, if they have extensive tidal flats and weaker friction, negative tidal asymmetry and a tendency to export sediments are observed. In short, tidal amplitude, lateral boundaries, bottom friction, and estuarine geometry are the factors that determine tidal asymmetry and the tendency to accumulate or export sediments or other materials, such as plastic debris.

Until now, studies have linked the origin of tidal asymmetry to non-linear tidal interactions in shallow waters. However, Hoitink et al. (2003) and Song et al. (2011) demonstrated that tidal asymmetry also arises in deep ocean waters because of interactions between some of the main tidal constituents. In addition, some research has highlighted the importance of ocean tidal asymmetry imposed at estuarine mouths in evaluating the deformation generated after tidal propagation and, consequently, determining estuarine morphological trends. Moore et al. (2009) found that the positive asymmetric character of the ocean tide at the mouth of the Dee Estuary (the UK) induced flood dominance, which explained the large-scale accretion that occurred over the last two centuries. Ranasinghe and Pattiaratchi (2000) found that the sediment export observed in three estuaries located on the southwestern coast of Australia could be explained by the negative tidal asymmetry at their mouths. Nidzieko (2010) investigated three Californian estuaries that also showed negative tidal asymmetry at their mouth; however, in these cases, the estuaries were characterized by very different geometric features, and the final asymmetric character depended both on the tidal asymmetry at the mouth and the estuarine geometry, especially regarding tidal flat extension. As the author concluded, tidal asymmetry develops with tidal propagation according to estuarine morphology, but tidal

© 2021. This manuscript version is made available under the CC-BY-NC-ND 4.0 license http://creativecommons.org/licenses/by-nc-nd/4.0/

asymmetry at the mouth must first be addressed.

From the information detailed above, the following conclusions can be drawn: just as tidal asymmetry is associated with sediment transport, it can be related to the transport of any other material, such as plastic debris; several studies have analysed the tidal deformation generated by tidal propagation through shallow waters and related this deformation with sediment transport and estuarine morphological trends; and finally, some authors have highlighted the relevance of the asymmetry imposed at estuarine mouths in the estuary-ocean flow exchange, tidal propagation, and, consequently, internal transport processes. However, to date, no general conclusions have been drawn regarding the effect of estuary geometry on an initially asymmetric tide at the mouth nor how this initial asymmetry affects the dispersion of materials in general or of plastic debris in particular.

This study explored as a novelty the relationship between the tidal deformation that arises from propagation, the initial asymmetry existing in estuarine mouths, and the morphological features of these environments. Furthermore, it contributes by assessing the effect of these interactions on the presence of plastic debris that reaches tidal estuaries from ocean sources. Although an important part of the plastic debris that is retained within estuaries comes from rivers (Rech et al., 2014), tide and waves also introduce them from sea-based sources (Hinojosa and Thiel, 2009). Because this study focused on exploring the role of the tide, the hydrodynamics of rivers, waves, and river sources were not included in the analyses. To achieve these objectives, a series of analyses based on the application of the hydrodynamic and particle tracking modules of the Delft3D numerical model (Hydraulics, 2018a,b; Roelvink and Van Banning, 1995) were conducted to study estuaries with different morphologies. The study estuaries were defined according

© 2021. This manuscript version is made available under the CC-BY-NC-ND 4.0 license http://creativecommons.org/licenses/by-nc-nd/4.0/

to the criteria of Speer and Aubrey (1985) and specifically correspond to tidal creeks. The high-resolution (1/30°) classification of ocean tidal asymmetry obtained by Núñez et al. (2020) was used to build the boundary conditions of the numerical models. The probabilistic analysis of the Lagrangian model allows us to draw some general considerations about the role of ocean tidal asymmetry and estuarine morphology on the presence of plastic debris within tidal estuaries. Furthermore, the application to a real estuary, the Pas Estuary (northern Spain) where field data on plastic debris are available, was also included to corroborate our findings.

The remainder of this paper is organized as follows: Section 2 describes the study estuaries, the astronomical tide dataset used to define the boundary conditions, and the setup of the numerical computations used in this research; Section 3 describes the main results; Section 4 details the application of our method to the Pas Estuary; Section 5 discusses the results of the developed research; and Section 6 outlines the main conclusions.

## 2. Material and methods

The proposed methodology used to assess the effect of ocean tidal asymmetry and estuarine morphology on tidal propagation and plastic debris presence within tidal estuaries is based on numerical simulations of a series of hydrodynamic and particle tracking scenarios in estuaries with different geometries. Fig. 1 shows an overview of the applied methodology.

© 2021. This manuscript version is made available under the CC-BY-NC-ND 4.0 license http://creativecommons.org/licenses/by-nc-nd/4.0/

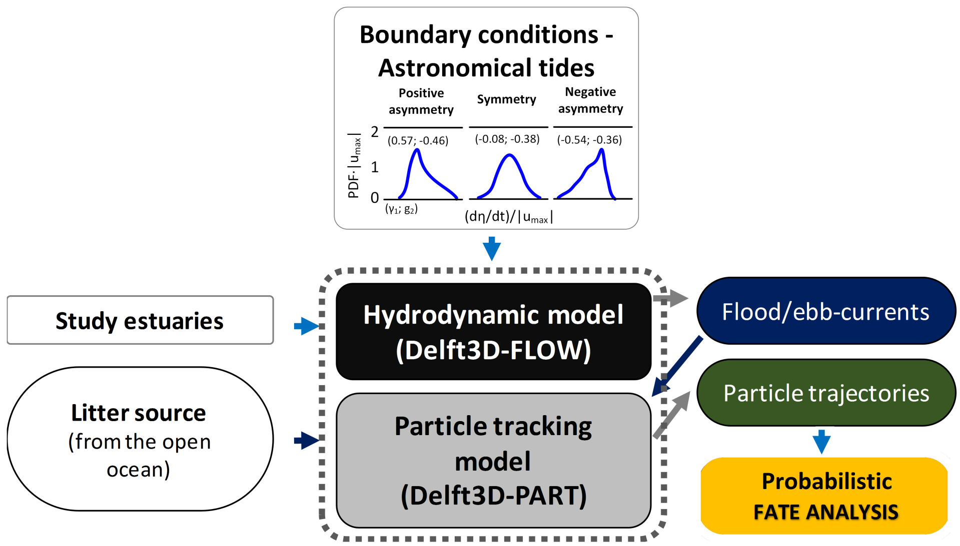


Figure 1: Flowchart of the model structure and data inputs and outputs.

The hydrodynamic (FLOW) and particle tracking (PART) modules of the Delft3D numerical model were applied offline to simulate plastic debris transport and fate within estuaries. Delft3D-FLOW (Hydraulics, 2018a; Roelvink and Van Banning, 1995) is an integrated flow modelling system that solves the Navier-Stokes equations for shallow water environments with the hypothesis of hydrostatic pressure and the Boussinesq approach. The model includes robust, accurate, and computationally efficient algorithms for simulating wetting-drying in intertidal flats (Lesser et al., 2004). Delft3D-PART (Hydraulics, 2018b) simulates material transport processes using forcings from the FLOW module and a particle tracking method based on a random walk method (Rubinstein and Kroese, 1981). Materials are represented by a set of particles characterised by a certain density. Delft3D-PAR enables the simulation of the transport of conservative substances by selecting the *tracer model* or hydrocarbons and their degradation processes

© 2021. This manuscript version is made available under the CC-BY-NC-ND 4.0 license http://creativecommons.org/licenses/by-nc-nd/4.0/

using the *oil model*. The *oil model* also allows us to consider the transport processes affected by wind drag additional advection or the beaching effect by defining a stickiness probability. The set of particles moves through the combined action of currents and wind (deterministic displacement) and turbulent diffusion (random displacement).

Delft3D is a widely applied state-of-the-art model used to evaluate different processes in complex estuarine systems. The Delft3D-FLOW module has been applied to several studies that have confirmed its ability to simulate hydrodynamics within estuaries (for example, Abascal et al., 2017; Bárcena et al., 2016; Iglesias and Carballo, 2010; García Alba et al., 2014; Jiménez et al., 2014; Núñez et al., 2019; Zhou et al., 2014). This and the possibilities offered by the Lagrangian module Delft3D-PAR to evaluate the transport of plastics (van Utenhove, 2019) have informed the selection of this model for this study.

### *2.1. Estuary configurations*

This study examines shallow well-mixed and tide-dominated estuaries with intertidal flats and submerged channels, where most water flows during ebb and flood phases. The shallow depths of the channels and tidal flats produce distinct tidal deformations, some of which can be detected with the naked eye.

To define the study estuaries, the criteria reported by Speer and Aubrey (1985) were used as references. These authors propose estuary analysis assuming a constant cross-sectional area in the longitudinal direction characterised by a main channel with a trapezoidal section and tidal flats. Four particular cases of this geometry were selected to describe different morphological features: a first estuary (EA) with a trapezoidal cross-sectional

© 2021. This manuscript version is made available under the CC-BY-NC-ND 4.0 license http://creativecommons.org/licenses/by-nc-nd/4.0/

area that is constant landward, a second estuary (EB) that is also constant landward but with a rectangular section, a third estuary (EC) whose trapezoidal section shows a linear reduction in depth toward its innermost areas, and a fourth estuary (ED) with a trapezoidal section that linearly reduces its width landward. While the EA and EB geometries show channelized geometries, EC and ED are more closely identified with common estuarine configurations. The dimensions, longitude ($L$), width ($b$), depth ($h$), and lateral slope of the channel ($N$) chosen for this study were within the ranges evaluated by Speer and Aubrey (1985) for shallow estuaries with long channels compared to their widths ($b/L << 1$) and small horizontal aspect ratios ($h/b << 1$). According to these geometries and dimensions, the study estuaries were classified as tidal creeks (Fig. 2).

© 2021. This manuscript version is made available under the CC-BY-NC-ND 4.0 license http://creativecommons.org/licenses/by-nc-nd/4.0/

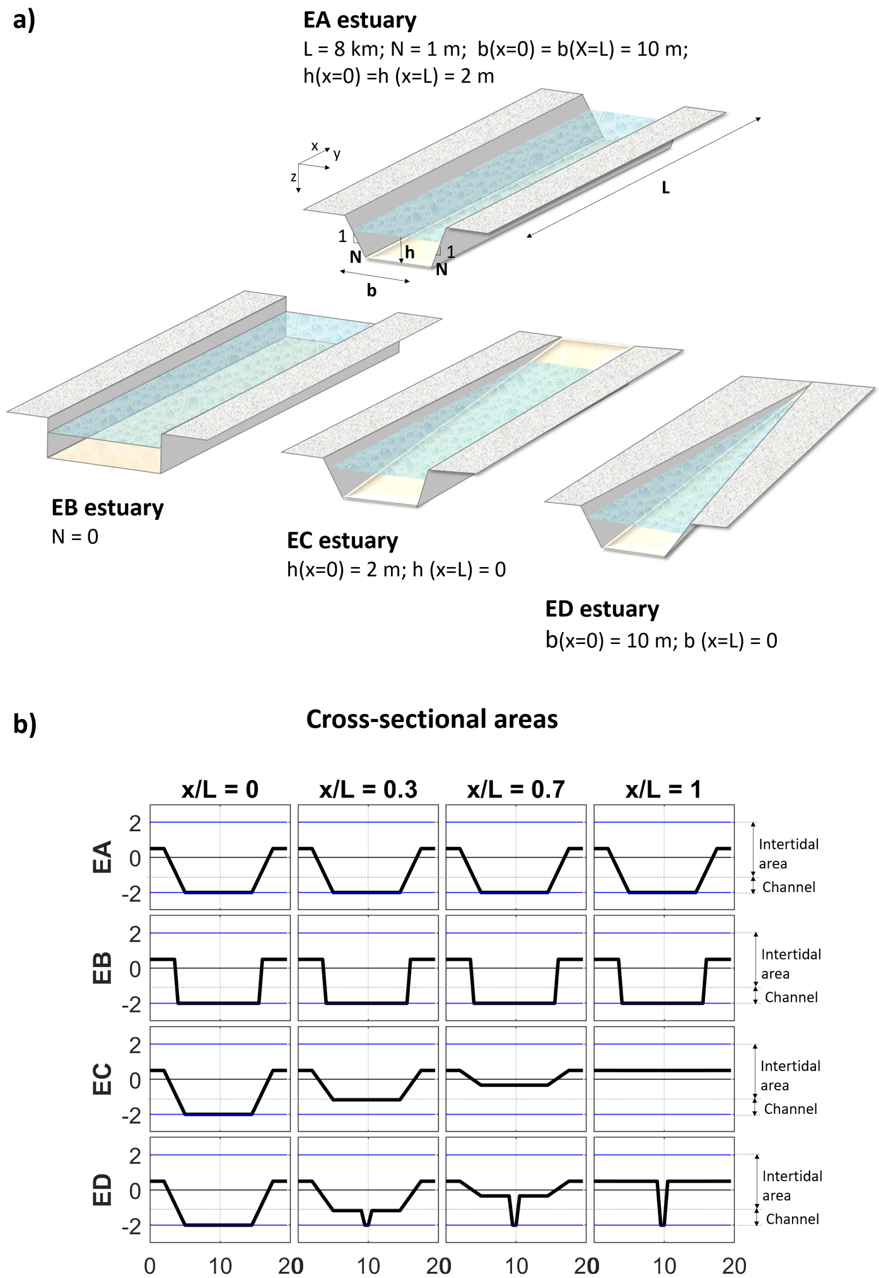


Figure 2: Geometry of the study estuaries: a) schemes with general dimensions and b) details of different cross sections. The mouth is located at $x/L = 0$, and the innermost area is located at $x/L = 1$.

© 2021. This manuscript version is made available under the CC-BY-NC-ND 4.0 license http://creativecommons.org/licenses/by-nc-nd/4.0/

### *2.2. Astronomical tide characterization*

The classification of astronomical tide on a global scale by Núñez et al. (2020) was used to characterise tidal asymmetry in estuarine mouths. This classification is based on the TPXO9-atlas barotropic tidal solution (Egbert and Erofeeva, 2002) and identifies, with a spatial resolution of 1/30° on the coastal areas, 25 representative astronomical tide types ($ATtypes$) globally according to their tidal asymmetry and periodicity parameters. Tidal asymmetry is described by the probability density functions (PDFs) of the tidal elevation time derivative, $d\eta/dt$ (a variable associated with the rising/falling tidal speeds and, therefore, with the flood/ebb currents in tidal estuaries), through the skewness ($\gamma_1$) and kurtosis ($g_2$) coefficients calculated from a 19-year series. Periodicity is defined by the tidal form factor and distinguishes semidiurnal, mixed-semidiurnal, mixed-diurnal, and diurnal regimes.

$\gamma_1$ of $d\eta/dt$ allows a relative comparison between flood and ebb current intensities, that is, it provides a measure of tidal current asymmetry and therefore provides information regarding the ability and orientation of the transport of materials (Nidzieko, 2010; Song et al., 2011). Positive values indicate that the flood-phase duration is shorter than the ebb-phase duration. As the tidal prism must remain the same, flood currents must be more intense than ebb currents, resulting in net transport towards the estuary. In contrast, if $\gamma_1$ is negative, ebb currents are the most intense and generate a trend of exporting materials to the open ocean. Núñez et al. (2020) proposed using the kurtosis ($g_2$) parameter together with $\gamma_1$, as $g_2$ compares the frequency of occurrence of the strongest flood/ebb currents (Balanda and MacGillivray, 1988; Westfall, 2014) and, consequently, is also related to the estuary capacity to transport materials. If the tides show a positive asymmetry, a lower kurtosis indicates a greater presence of stronger flood

© 2021. This manuscript version is made available under the CC-BY-NC-ND 4.0 license http://creativecommons.org/licenses/by-nc-nd/4.0/

currents, and this aspect can be associated with a greater tendency to import materials. In contrast, if the tides are negatively asymmetric, a lower kurtosis indicates a greater frequency of stronger ebb currents. The set of $\gamma_1$ and $g_2$ obtained for a specific time period explains the residual currents for such period, as their magnitudes and directions are strongly conditioned both by the value of the maximum flood/ebb currents and their frequency of occurrence. Residual currents in tidal estuaries are key factors that influence transport processes (Carmo et al., 2010; Feng et al., 1986).

### *2.3. Hydrodynamic model*

As the study estuaries are shallow, narrow, and tidal estuaries, that is, tidal creeks, and the astronomical tide is the only analysed driver, 2D hydrodynamic modelling is suitable for representing the flow features. The hydrodynamic grids used to numerically evaluate the above-described estuaries have 160000 computational elements and an average spatial resolution of 1 m, which is suitable for describing the hydrodynamic and transport processes at these spatial scales.

In this study, to assess the role of different tidal asymmetric natures, three $ATtypes$ with different $\gamma_1$ and similar $g_2$ values were selected as the analysis tides. The selected types were $ATtype_1$ ($\gamma_1$ = 0.57), $ATtype_{16}$ ($\gamma_1$ = -0.08), and $ATtype_{24}$ ($\gamma_1$ = -0.54), all of which show $g_2$ values of approximately -0.4. $ATtype_1$ is a positive asymmetric tidal type. Positive asymmetric tides are representative of 11.3% of the world's coastal areas, such as the western Gulf of Mexico, northern Caribbean Sea, Mediterranean coast of France, and south coast of Australia, as well as part of the Spanish coast, and conditions the behaviour of the estuaries they house. $ATtype_{16}$ is associated with the symmetric tides. Symmetric tides are present in 77.4%

© 2021. This manuscript version is made available under the CC-BY-NC-ND 4.0 license http://creativecommons.org/licenses/by-nc-nd/4.0/

of coastal areas of the world. A significant part of the coastal areas of the Atlantic Ocean, including the East Coast of the USA, the western coast of Spain, and large proportions of the Brazilian and African coasts, exhibit symmetric tides. Within the group of symmetric tides classified by Núñez et al. (2020), those with bimodal PDFs of $d\eta/dt$ show the most widespread presence (47.4% of the world's coastal areas), $ATtype_{16}$, which shows a unimodal PDF (see Fig. 3), was selected for this study. The reason is the interest in evaluating the behaviour of tides that differ only in their tidal skewness. $ATtype_{16}$ allows the selection of a symmetric tide type while keeping the other parameters, such as kurtosis, similar to the other two selected tidal types. Symmetric tides with unimodal PDFs represent 30% of coastal areas in the world. Finally, $ATtype_{24}$ refers to negative asymmetric tides, which are found in the remaining 11.3% of coastal areas. Negative tides can be found in coastal areas located in the southern Caribbean Sea, northern Greenland, the South China Sea, and western Australia (Núñez et al., 2020). Consequently, the importance of evaluating the influence of these tidal types is demonstrated, as they are the tidal types that can be found on the mouths of estuaries located in different areas worldwide and influence their internal processes. Fig. 3 shows the standardized (between -1 and 1 values) PDFs of $d\eta/dt$ associated with the positive asymmetric tide $ATtype_1$, the symmetric tide $ATtype_{16}$, and the negative asymmetric tide $ATtype_{24}$, as well as the 15 daily water level conditions from such tidal types.

The analysis period was set to 15 days to contemplate the residual transport caused by the complete neap-spring tidal cycles. The analysis time period is shown in Fig. 3 between two vertical red lines. Furthermore, to avoid the effect of different potential tidal ranges on the fate of plastic debris

© 2021. This manuscript version is made available under the CC-BY-NC-ND 4.0 license http://creativecommons.org/licenses/by-nc-nd/4.0/

within estuaries and analyse the effects of tidal asymmetry and estuarine geometry only, the tidal series were standardised so that the maximum tidal amplitude took a unit value. Similarly, to obviate the effect of plastic debris inputs reaching estuaries at different tidal phases associated with different tidal ranges, it is assumed that the plastic debris reaches estuaries at low tide with a mean tidal range of 1 m in all cases. Therefore, the boundary conditions were the 15-daily time series of astronomical tides with a 10-min temporal resolution associated with the tidal types ($ATtypes_i$, where i = 1, 16, and 24). The initial conditions of the analysis correspond to 10 min after the low tide level, when the estuary begins to flood.

To evaluate the 2D hydrodynamics in the study estuaries, the roughness coefficients ($C$) and horizontal eddy viscosities ($\epsilon$) were defined. $C$ was characterised as a variable with depth according to the equivalent geometrical roughness of Nikuradse ($k_s$), and $\epsilon$ varied with cell size according to a calibration constant ($k$). Considering that both the geometries and the representative dimensions of the study estuaries were within the ranges evaluated by Speer and Aubrey (1985) and Bárcena et al. (2016), these parameters were consistently defined for all study estuaries by adopting a value of 0.2, for $k_s$ and 0.1, for $k$.

The flood/ebb currents for the selected tidal types (positive asymmetric, symmetric, and negative asymmetric) and for the defined estuaries (EA, EB, EC, and ED) were obtained by applying the above-described models.

© 2021. This manuscript version is made available under the CC-BY-NC-ND 4.0 license http://creativecommons.org/licenses/by-nc-nd/4.0/

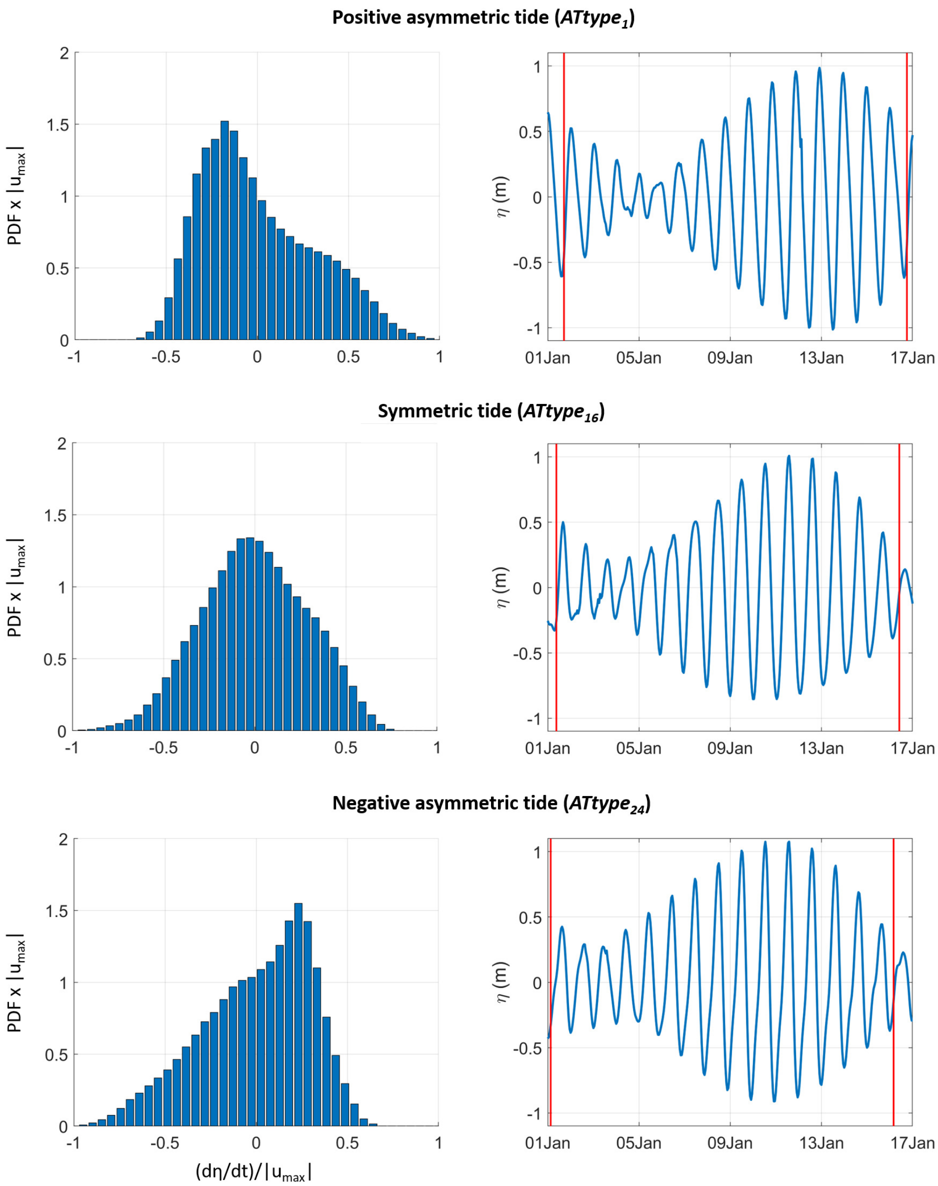


Figure 3: Tidal types for analysis and associated boundary and initial conditions.

© 2021. This manuscript version is made available under the CC-BY-NC-ND 4.0 license http://creativecommons.org/licenses/by-nc-nd/4.0/

### *2.4. Particle tracking model*

The simulated high-resolution flood/ebb currents were the inputs of the Delft3D-PAR module. The *oil model* was selected to include the beaching effect in plastic debris transport simulations. Owing to the current limited knowledge about the interaction between plastic debris and shoreline and to assess the presence of plastic from a hydrodynamic perspective, a simplified beaching effect was defined (Núñez et al., 2019). A small stickiness probability of 0.5% favours the presence of free particles throughout the entire simulation, which is useful for considering the influence on transport of the complete neap-spring cycle and allows particles to be trapped by the shoreline. Following van Utenhove (2019), the oil degradation processes were neglected, and the only processes considered were advective transport due to tidal currents and diffusive transport. The diffusion coefficient ($D$) was set to 1 $m^2/s$, which is suitable for estuarine areas (Abascal et al., 2017, 2012; Núñez et al., 2019; Viikmäe et al., 2013).

Considering that one of the most common plastics found in the marine environment is polypropylene (Mazarrasa et al., 2019; Zhang, 2017), this study represented plastic debris with particles of 0.89 $g/cm^3$ of average density. Furthermore, it was assumed that these particles were always floating and were transported over the surface, that is, the settling velocity was set to zero. The origin of plastic debris was assumed to be marine; the debris reached the estuarine mouths at the low tide with a mean tidal range of 1 m for all assessed scenarios. Regarding the number of particles, there is a large variability in the selection of the number of particles in the literature as a function of the extension of the study area. Studies such as Abascal et al. (2009); Barker and Galt (2000); Díaz et al. (2008); Núñez et al. (2019), and van Utenhove (2019) have shown that thousands of particles per location

© 2021. This manuscript version is made available under the CC-BY-NC-ND 4.0 license http://creativecommons.org/licenses/by-nc-nd/4.0/

may be sufficient on regional and local spatial scales. In this study, 100 times greater order of magnitude was chosen to ensure the accuracy and robustness of the probability analyses derived from this study. Regarding the time step ($\Delta t$), 5 min was adopted to ensure the stability of the model.

Particle trajectories for the four study estuaries forced with the three tidal types were obtained using the particle tracking model with the aforementioned setup.

### *2.5. Probabilistic analysis*

A probabilistic analysis of the particle trajectories obtained from Delft3D-PAR determined the most likely areas, defined according to their distance to the mouth, of plastic debris presence for the selected time horizon of 15 days. In this period, because of the defined beaching features, most particles have not yet been retained by the coast, but they continue to move immersed in the tidal flow. For this reason, the average probability of the presence of particles over a neap-spring tidal cycle, which includes the effect of tidal hydrodynamic variability during the analysis period, was used as the analysis variable (Abascal et al., 2010). Thus, the effects of the uncertainties associated with some of the assumed hypotheses, such as the origin of plastic debris or the tidal phase in which plastic debris reaches the estuary, can be mitigated.

To perform these probabilistic analyses, the study estuaries were discretized into $N_{CS}$ estuarine units (sections) in the longitudinal direction of the estuary. Twenty ($N_{CS}$) sections 400 m in length were found to be suitable for characterising the plastic distribution of the estuaries analysed. For each of these sections ($j$), the average probability of the presence of particles

© 2021. This manuscript version is made available under the CC-BY-NC-ND 4.0 license http://creativecommons.org/licenses/by-nc-nd/4.0/

in a neap-spring tidal cycle ($P_m$) was calculated (Eq. 1).

$$P_{mj} = n_j/N_T \times 100 \tag{1}$$

where $n_j$ is the average number of particles in section $j$ in a neap-spring tidal cycle, and $N_T$ is the total number of evaluated particles, that is, 100000 particles.

Moreover, to check whether an estuary with a certain tidal asymmetry imposed at its mouth shows a trend of importing particles, the sum of $P_{mj}$ in all estuarine units was calculated ($P_m = \sum_{j=1}^{N_{CS}} P_{mj}$).

## 3. Results

### *3.1. Effects of tidal asymmetry and estuarine morphology on tidal propagation*

Fig 4 shows the evolution of the skewness ($\gamma_1$) and kurtosis ($g_2$) coefficients of the 15-daily $d\eta/dt$ when the three analysed tidal types propagate by each of the four estuaries studied.

© 2021. This manuscript version is made available under the CC-BY-NC-ND 4.0 license http://creativecommons.org/licenses/by-nc-nd/4.0/

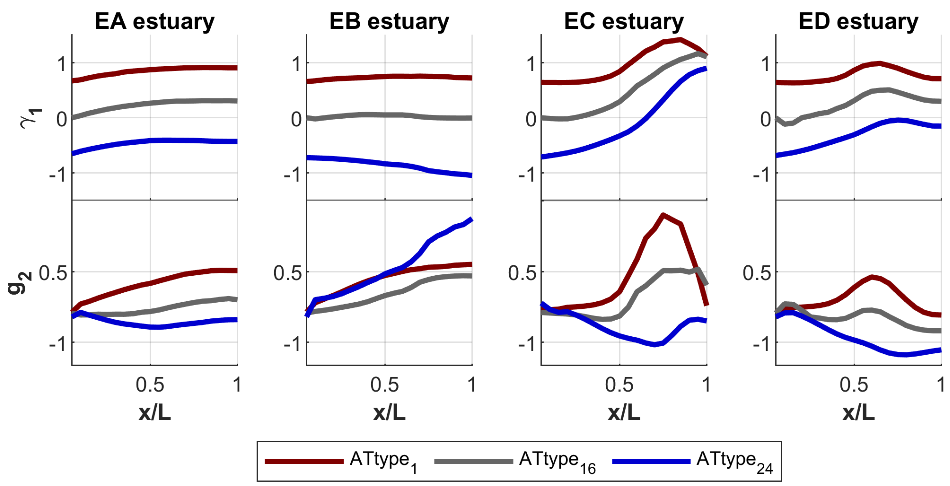


Figure 4: Skewness ($\gamma_1$) and kurtosis ($g_2$) coefficients of $ATtype_1$, $ATtype_{16}$, and $ATtype_{24}$ along the EA, EB, EC, and ED channels.

The effect of the lateral boundary inclination of the channel on tidal propagation was deduced by comparing the hydrodynamic results in EA and EB estuaries. The lateral boundaries of the channel oppose tidal flow. A greater inclination translates into greater friction, which is more noticeable at low tide than at high tide, delaying the ebb tide and generating a deformation with a flood-dominance trend ($\gamma_1$ increases). However, the flood- or ebb-dominant nature depends not only on the geometry but also on the ocean tidal asymmetry imposed at the estuarine mouths. Within the EA estuary, which is characterised by a 45° inclination at its lateral boundaries, $\gamma_1$ gradually increases to the middle of the estuary for the three tidal types analysed; however, the change is not very significant in the inner half. Thus, the positive asymmetry existing at the mouth for $ATtype_1$ increases, the symmetric tide of $ATtype_{16}$ is transformed into a positive asymmetric tide, and the initial negative asymmetry of $ATtype_{24}$ is reduced. The

© 2021. This manuscript version is made available under the CC-BY-NC-ND 4.0 license http://creativecommons.org/licenses/by-nc-nd/4.0/

configuration of the EB estuary with vertical lateral boundaries generates little opposition to the tidal flow, such that the induced changes in $\gamma_1$ are not very relevant for the positive asymmetric and symmetric tides, and the (a)symmetries of the mouth are maintained. Furthermore, this geometry can generate an opposite effect ($\gamma_1$ reduces) on initially deformed tides with negative asymmetry, favouring an even faster ebb phase and increasing the initial ebb dominance. Regarding the kurtosis spatial evolution, $g_2$ increases as tides become more asymmetric, either positive or negative, and vice versa. Hence, the most intense flood or ebb currents decrease their frequencies in favour of average currents for positive and negative asymmetric tides, respectively, when $g_2$ increases and vice versa when $g_2$ decreases. A decrease in $g_2$ is observed for $ATtype_{24}$ in the outer half of the EA estuary when the negative asymmetric character is reduced. This translates to an increase in the frequency of the strongest ebb currents in this area. In the EA estuary, $g_2$ always reaches lower values than in the EB estuary for all analysed sections, which means that the strongest tidal currents are more frequent within the EA geometries than within the EB geometries. In summary, greater inclinations of the lateral boundaries of the channel increase the positive tidal asymmetry and counteract the negative asymmetry; however, the final asymmetric character of the tide in the innermost sections is not determined by this geometric aspect but rather by the initial tidal asymmetry shown at the mouth. Furthermore, friction related to lateral boundaries increases the frequency of flood/ebb currents for positive/negative asymmetric tides.

The effect of depth reduction in the three analysed tidal types is described from the hydrodynamics obtained for the EA and EC estuaries. The EC shows a linear reduction in depth in its longitudinal direction with respect to the EA estuary. This reduction implies an increase in friction

© 2021. This manuscript version is made available under the CC-BY-NC-ND 4.0 license http://creativecommons.org/licenses/by-nc-nd/4.0/

that slows down the ebb phase for all the analysed tides and stores a higher intertidal water volume in its innermost area. It is worth noting a different behaviour in the EC estuary between the outer and intermediate areas, where the depth allows the full development of every tidal range, and the innermost area, where flooding-drying processes take place. Thus, in the outer half of the estuary, the positive growth of the skew for every tidal type is slow and gradual, analogous to that experienced in estuary EA. This translates into similar effects of both types of estuaries on tidal asymmetry. However, while this positive trend stabilises in the second half of the EA estuary, it grows faster in the EC estuary due to a more evident bottom effect. This growth continues until reaching a maximum—approximately 75% of the estuary length for $ATtype_1$ and near the final section for $ATtype_{16}$ and $ATtype_{24}$—from this point on, a nonsignificant decay is observed, which is probably due to intertidal storage in these areas. Indeed, the asymmetry of all the analysed tides results in positive asymmetry in the interior areas of the EC estuary, and $\gamma_1$ always takes higher values than in the EA estuary. With regard to $g_2$ in the outer half of the EC estuary, significant changes are only observed for $ATtype_{24}$, where a decrease in $g_2$, that is, an increase in the frequency of occurrence of the most intense ebb currents occurs while reducing the negative asymmetric nature of the tide. In this outer area, $g_2$ always adopts lower values in the EC estuary than in the EA estuary. In the interior areas of the EC estuary, $g_2$ is lower than in the same areas of the EA estuary only for $ATtype_{24}$, but it adopts higher values for $ATtype_1$ and $ATtype_{16}$. Therefore, it is deduced that the longitudinal depth reduction leads to a positive tidal asymmetric character in the interior areas, regardless of the initial asymmetry at the mouth. Nevertheless, the intertidal storage in the innermost areas slows the flood-current velocities and compensates

© 2021. This manuscript version is made available under the CC-BY-NC-ND 4.0 license http://creativecommons.org/licenses/by-nc-nd/4.0/

for the positive increase in tidal asymmetry.

The channel-width variation effect on tidal propagation was explained by contrasting the results obtained for the EA and ED estuaries. Unlike the EA estuary, the ED estuary shows a linear reduction in the width of its channel that reaches zero in its innermost area. The behaviour of the tides is similar in both estuaries, up to approximately half their lengths. In these areas, a positive asymmetry ($\gamma_1 > 0$) is induced by friction related to the lateral boundaries of the channels. This positive asymmetry adds, for $ATtype_1$ and $ATtype_{16}$, or counteract, for $ATtype_{24}$, the initial asymmetry that is present at the mouth. As mentioned, the asymmetry of the analysed tides in the EA estuary remains practically constant in its innermost area, while negative asymmetry is induced in the ED estuary ($\gamma_1 < 0$). This can be explained by two factors related to the morphological configuration of the ED estuary. On the one hand, the gradual narrowing of the section reduces the inclination of the lateral boundaries of the channel, which becomes practically vertical slightly beyond the middle of the estuary, and reduces the friction. On the other hand, the area of the tidal flat increases in the innermost area of the estuary ED, thereby favouring intertidal storage and counteracting the deformation induced by the channel. However, as shown in Fig. 4, the final $\gamma_1$ value depends both on the initial value of ocean tidal asymmetry and on the estuarine morphology. Regarding $g_2$, the maximum values reached in the ED estuary for the three tides were always lower than those reached in the EA estuary. Therefore, it can be deduced that a reduction in the channel section increases the frequency of stronger tidal currents.

Fig. 5a shows the residual current maps obtained for each estuary and tide in the analysed neap-spring cycles. A series of significant aspects can be drawn from this figure. On the one hand, the external tidal asymmetry plays

© 2021. This manuscript version is made available under the CC-BY-NC-ND 4.0 license http://creativecommons.org/licenses/by-nc-nd/4.0/

a major role on the residual current patterns within tidal estuaries. In general, an external positive asymmetry favours flood residual currents, whereas symmetric and negative asymmetric tides promote ebb residual currents. Furthermore, as can be inferred from the comparisons of residual currents of EA and EB estuaries, a greater friction related to the lateral boundaries of the channel derives a flood trend. On the contrary, an intertidal storage in tidal flats causes small residual currents over these areas and favours ebb residual currents through the channels (compare residual currents in EA with EC and ED estuaries). Fig. 5b shows the relationship between the residual currents of the central longitudinal section of estuaries and the pair $\gamma_1$ - $g_2$. The highest residual currents in the flood/ebb direction are achieved in a balance between the highest absolute value of $\gamma_1$—a greater difference between the flood and ebb current intensity—and the smallest value of $g_2$—a greater relative frequency of the strongest currents. However, if tide at the mouth is symmetric (near-zero $\gamma_1$) and $g_2$ is less than zero, ebb residual currents are induced.

© 2021. This manuscript version is made available under the CC-BY-NC-ND 4.0 license http://creativecommons.org/licenses/by-nc-nd/4.0/

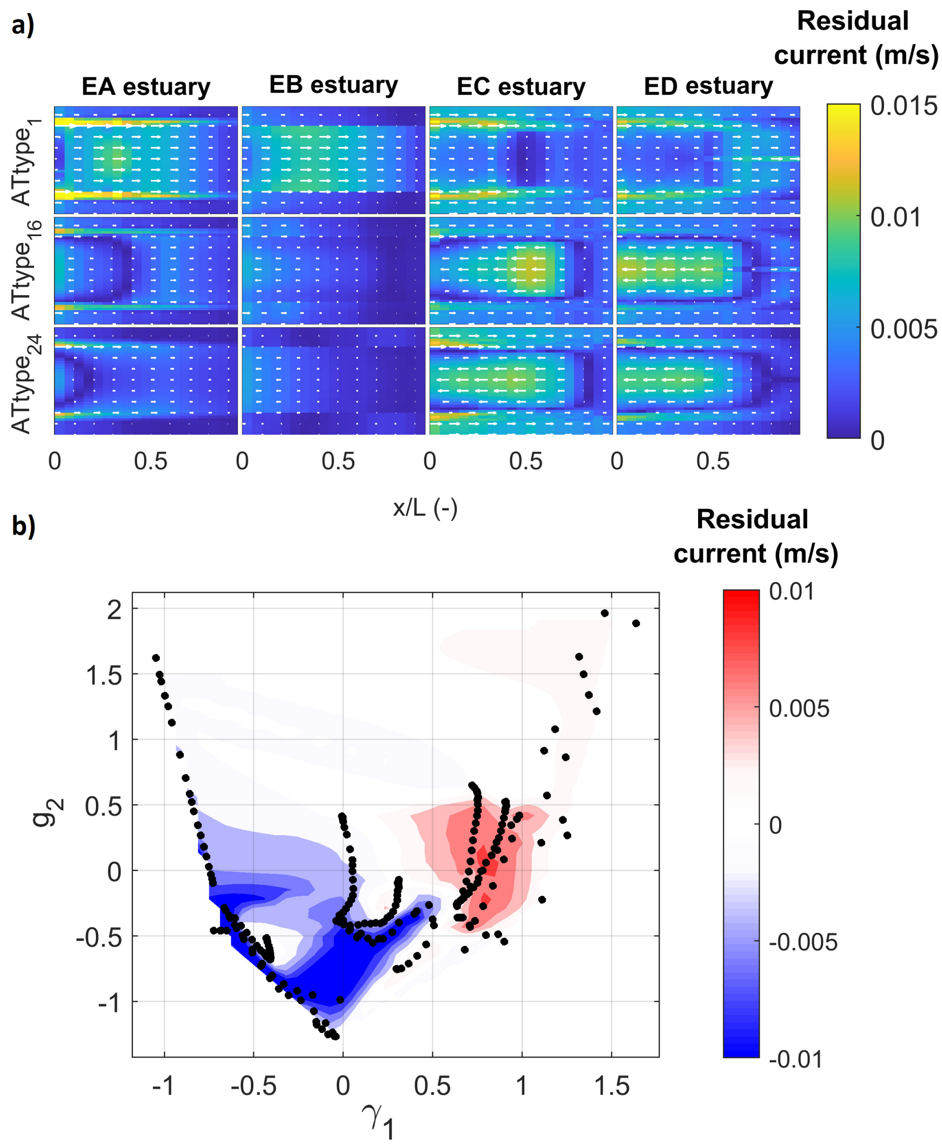


Figure 5: 15-day residual currents of $ATtype_1$, $ATtype_{16}$, and $ATtype_{24}$ along the EA, EB, EC, and ED estuaries (a) and relationship between residual currents and the pair $\gamma_1$-$g_2$ (b).

© 2021. This manuscript version is made available under the CC-BY-NC-ND 4.0 license http://creativecommons.org/licenses/by-nc-nd/4.0/

Figs. 4 and 5 reveal several significant aspects. On the one hand, a greater friction associated with the lateral boundaries or the bottom of the channel produces a positive asymmetric trend, increases the occurrence of the strongest tidal currents and, in general, favours the flood residual currents. However, a weaker friction or a significant storage capacity in the intertidal flats can generate a negative asymmetric trend, reduce the frequency of the strongest currents, and favour ebb residual currents. In general, due to changes in tidal phase durations, the frequency of the strongest tidal current in the direction of asymmetry decreases as the tide becomes more asymmetric and increases otherwise.

### *3.2. Effects of tidal asymmetry and estuarine morphology on the fate of plastic debris*

Fig. 6 shows an example of the temporal evolution of $P_m$ over the analysed neap-spring cycle of the symmetric tide ($ATtype_{16}$) for different sections of the EA estuary ranging from the mouth ($x/L = 0$) to its innermost area ($x/L = 1$). The evolution of the average probability of the plastic presence in each section is explained by the marine origin assumed for the plastic debris. A high probability of plastic debris presence is found in the sections between the mouth and approximately the middle of the estuary during the first days of the neap-spring cycle, when the particles reach the estuary and begin to be transported. In contrast, an average probability of presence of plastic higher than zero begins to appear in the innermost sections of the estuary after day 10 of the tidal cycle. This implies that the plastic debris that reach the mouth of the EA estuary during the low tide of a symmetric tide do not reach the interior areas after 10 days.

© 2021. This manuscript version is made available under the CC-BY-NC-ND 4.0 license http://creativecommons.org/licenses/by-nc-nd/4.0/

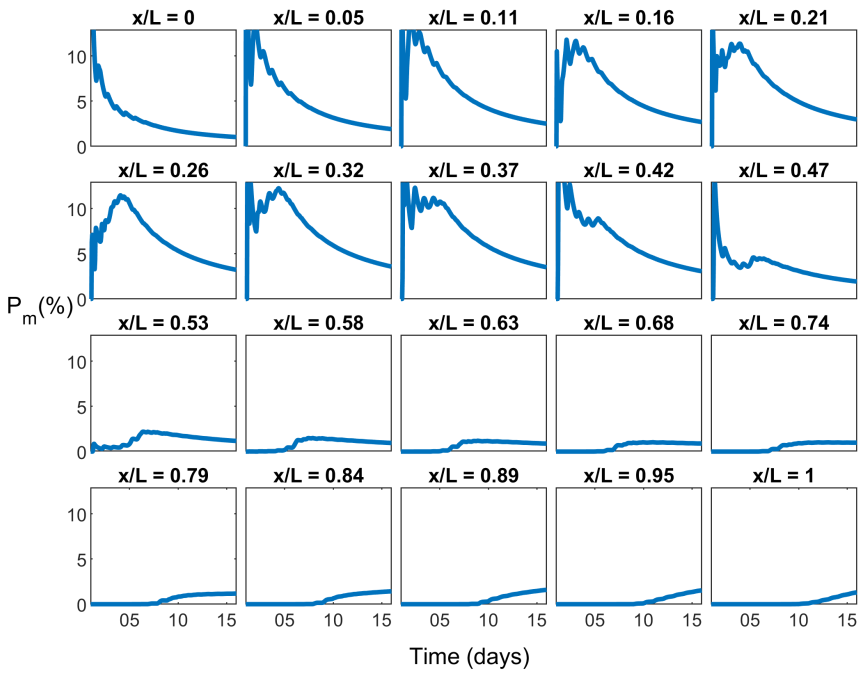


Figure 6: Temporal evolution of $P_m$ from the mouth of the EA estuary ($x/L = 0$) to the innermost area ($x/L = 1$).

The $P_m$ values of the estuarine sections on day 15 of the tidal cycle were used to reconstruct the distribution of the average probability of the presence of particles within the neap-spring cycle along the estuaries. Fig. 7 shows these $P_m$ distributions (grey areas) and the percentage of particles trapped on the shoreline, $P_s$ (red lines) at the end of the simulations for each estuary and tide. Table 1 includes the sum of $P_m$ and $P_s$ for the analysed estuaries.

© 2021. This manuscript version is made available under the CC-BY-NC-ND 4.0 license http://creativecommons.org/licenses/by-nc-nd/4.0/

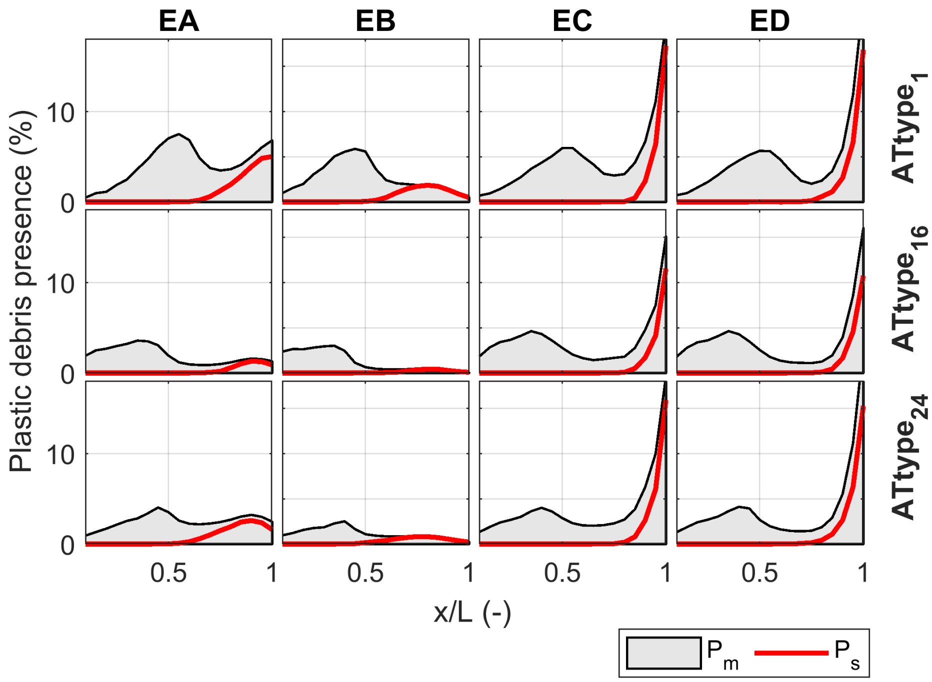


Figure 7: Average probability of the presence of particles $P_m$ (grey area) in a neap-spring tidal cycle and percentage of particles trapped on the shoreline $P_s$ (red line) at the end of the tidal cycle.

© 2021. This manuscript version is made available under the CC-BY-NC-ND 4.0 license http://creativecommons.org/licenses/by-nc-nd/4.0/

| | $\sum P_m(\%)$ | | | | $\sum P_s(\%)$ | | | |
|---|---|---|---|---|---|---|---|---|
| | $EA$ | $EB$ | $EC$ | $ED$ | $EA$ | $EB$ | $EC$ | $ED$ |
| $ATtype_1$ | 81 | 52 | 93 | 92 | 21 | 11 | 28 | 29 |
| $ATtype_{16}$ | 38 | 25 | 72 | 70 | 5 | 2 | 19 | 18 |
| $ATtype_{24}$ | 49 | 23 | 78 | 78 | 15 | 6 | 27 | 27 |

Table 1: $\sum P_m$ and $\sum P_s$ within the EA, EB, EC, and ED estuaries for $ATtype_1$, $ATtype_{16}$, and $ATtype_{24}$.

The results are shown in Fig. 7 and Table 1 indicate that the ocean tidal asymmetry significantly conditions the ability to import plastic debris in channelized geometries, such as the EA estuary. With the propagation of positive asymmetric tides, the EA estuary shows a clear presence of particles ($\sum P_m^{ATtype_1} = 81\%$) for the 15 days analysed, revealing a greater probability of presence in the vicinity of the middle and final sections of the estuary ($P_m^{ATtype_1}$ in $x/L$ near 0.5, and 1 is close to 8%). This distribution of the peak probabilities is equivalent for symmetric and negative asymmetric tides, but in these cases, the peaks are located in slightly forward positions, and the magnitude is significantly reduced ($P_m^{ATtype_{16}}$ and $P_m^{ATtype_{24}} < 4\%$ at the peaks). In both cases, the average presence of plastic debris was reduced to approximately 38% ($\sum P_m^{ATtype_{16}}$) and 49% ($\sum P_m^{ATtype_{24}}$). For the three tides analysed, most particles located within the EA estuary moved by hydrodynamics at the end of the simulations. The percentages of trapped particles ($P_s$) represent 21%, 5%, and 15% of the total for $ATtype_1$, $ATtype_{16}$, and $ATtype_{24}$, respectively. The accumulation occurs from $x/L$ equal to 0.5 and reaches its maximum value (5% for $ATtype_1$ and approximately 2% for

© 2021. This manuscript version is made available under the CC-BY-NC-ND 4.0 license http://creativecommons.org/licenses/by-nc-nd/4.0/

$ATtype_{16}$ and $ATtype_{24}$) in the innermost estuarine section. As the stickiness probability was defined with the same value along the entire shoreline, the distribution of the trapped particles can be explained by the residual currents reflected in Fig. 5a. Thus, in the EA estuary, the flood residual currents generated by $ATtype_1$ reach their maximum value—which oscillates between 0.01 and 0.015 m/s—in $x/L$ equal to 0.5. This current generates a landward residual transport of plastic debris which reaches the innermost area of the estuary to be retained ($\sum P_s$ of 21%). $ATtype_{16}$ generates ebb residual currents that reach 0.01 m/s at the mouth ($x/L < 0.5$) and therefore induces seaward transport in this area. The plastic debris remaining in the inner half of the estuary is transported landward by the flood residual currents, which oscillate around 0.004 m/s, and it is accumulated ($\sum P_s$ of 5%). $ATtype_{24}$ produces a residual current pattern such as $ATtype_{16}$, except that the ebb currents are limited to the section $0 < x/L < 0.25$ and their maximum magnitude is 0.005 m/s. Therefore, $ATtype_{24}$ results in less residual loss than $ATtype_{16}$ and a greater accumulation of plastic debris ($\sum P_s$ of 15%).

As in the EA estuary, the presence of plastic debris within the EB estuary is strongly conditioned by the asymmetry of the ocean tide. However, the EB estuary shows the lowest capacity to import floating items due to flood/ebb currents. The average probability of presence does not exceed 52% for positive asymmetric tides ($ATtype_1$), 25% for symmetric tides ($ATtype_{16}$), and 23% for negative asymmetric tides ($ATtype_{24}$). Regarding the $P_m$ distribution along the longitudinal profile of the estuary, common patterns that differed in magnitude depending on the tidal type propagated were observed. Thus, an increasing cumulative trend between the mouth and the middle section of the estuary was observed for all analysed tidal

© 2021. This manuscript version is made available under the CC-BY-NC-ND 4.0 license http://creativecommons.org/licenses/by-nc-nd/4.0/

types, and from this area, a significant reduction in the value of $P_m$ is observed. Regarding the accumulation, it is worth highlighting only the one produced in the inner half of the estuary because of the flood residual currents of $ATtype_1$ (0.008 m/s drives $\sum P_s$ around 11%). As $ATtype_{16}$ and $ATtype_{24}$ show ebb residual currents for the entire estuary, where the highest intensities are 0.005 m/s and occur in the vicinity of the mouth, the trend does not accumulate ($\sum P_s$ lower than 6%).

The geometries of EA and EB represent idealised channels where the probability of plastic debris presence and accumulation depends both on the initial tidal asymmetry at the mouths and the friction associated with the lateral boundaries.

The geometries of the EC and ED describe estuaries with common morphological configurations. The $P_m$ and $P_s$ results from these geometries show that the distributions of plastic debris are very similar and that these typologies of tidal estuaries frequently act as traps for plastic debris, regardless of tidal asymmetry. Indeed, both EC and ED estuaries show an average probability of plastic debris presence greater than 90% for the positive asymmetric tide $ATtype_1$, approximately 70% for the symmetric tide $ATtype_{16}$, and close to 80% for the negative asymmetric tide $ATtype_{24}$. The longitudinal distribution of $P_m$ in these estuaries shows a relative peak close to 5% around the middle of the estuary and an absolute peak at approximately 20% in the innermost area. Furthermore, in all cases and in just 15 days, approximately between 20% and 30% of the particles were trapped in the innermost tidal flats, where residual currents were lower due to intertidal storage ($< 0.002$ m/s).

© 2021. This manuscript version is made available under the CC-BY-NC-ND 4.0 license http://creativecommons.org/licenses/by-nc-nd/4.0/

## 4. Application to the Pas Estuary

### *4.1. Study site and data*

The Pas Estuary flows into the Cantabrian Sea in the Gulf of Biscay, northern Spain (Fig. 8a). The Pas Estuary is a shallow well-mixed estuary, where the key driver of hydrodynamics and transport is the astronomical tide (Galván et al., 2010). The tide in this area corresponds to the $ATtype_{14}$ of the astronomical tide classification by (Núñez et al., 2020) (Fig. 8c). The tide is symmetric with neap, mean and spring tidal ranges of approximately 1.5, 2.8, and 4.5 m, respectively, and a tidal prism ($\Omega$) of $4.8 \times 10^6$ m$^3$. Fluvial currents are negligible compared to tidal currents (García et al., 2008; Galván et al., 2010).

The Pas Estuary shows an elongated shape with a NW-SE alignment of approximately 8 km in length and a landward reduction of the channel section from the mouth, where the width is approximately 300 m, to the limit of the tidal influence, where the width is 50 m. Its depth is reduced from 2 m at the mouth to approximately 1 m at its innermost area. The tidal flats represent approximately 60% of the estuary and are mainly located in the outer left area. Therefore, the Pas Estuary shows an intermediate geometry between the previous EC and ED estuaries. The main differences are the curves of the main channel and the location of the tidal flats, as they are in the outermost area of the Pas Estuary, but they are in the inner half of the EC and ED estuaries.

© 2021. This manuscript version is made available under the CC-BY-NC-ND 4.0 license http://creativecommons.org/licenses/by-nc-nd/4.0/

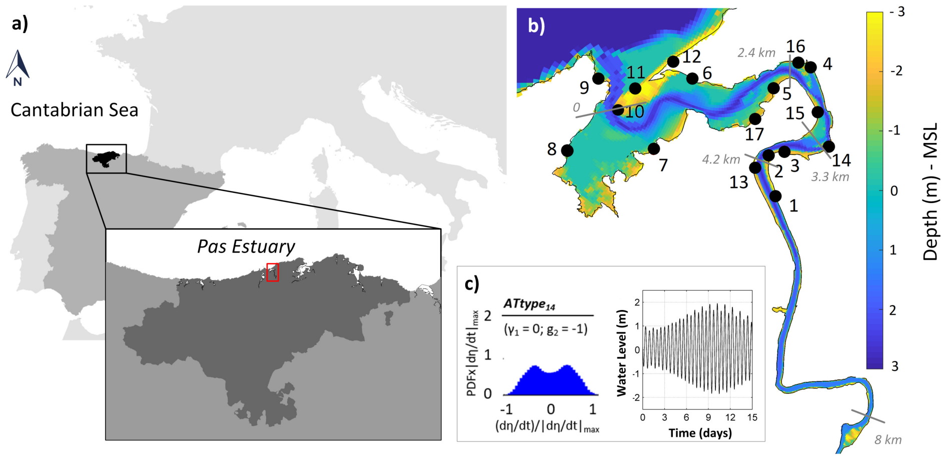


Figure 8: Pas Estuary: a) location, b) bathymetry and data points with average density (AD) of plastic debris ($i = 1, 2, ..., 17$), and c) representative tidal type and associated water level.

*Bathymetric data*

In the Pas Estuary, the areas above mean sea level (MSL) were defined with topographic data LIDAR (2012), from the Spanish National Geographic Institute (`http://centrodedescargas.cnig.es/CentroDescargas/`), with a density of 0.5 points/m and an altitude accuracy of 20 cm. Depths located below the MSL were obtained from the Nautical Chart 939 (Spanish Navy Hydrography Office, IHM) (see Fig. 8b).

*Plastic debris density data*

In the Pas Estuary, plastic debris density data are available from a marine litter field survey performed between March 2017 and October 2017 and in 17 sampling areas (Fig. 8b) (Mazarrasa et al., 2019).

© 2021. This manuscript version is made available under the CC-BY-NC-ND 4.0 license http://creativecommons.org/licenses/by-nc-nd/4.0/

### *4.2. Numerical model setup*

As the Pas Estuary is a well-mixed estuary, 2D hydrodynamic modelling is suitable for representing flow features. The Pas Estuary was represented by a curvilinear grid covering the estuarine area with hydrodynamic continuity. The grid is composed of 463 $\times$ 85 elements and shows a variable resolution between 190 m in the outer boundary and 8 m in the inner estuarine area. The roughness coefficient ($C$) and the horizontal eddy viscosity ($\epsilon$) are defined as in Subsection 2.3 because they correspond to the common values associated with the estuaries of the north coast of Spain (for example, Bárcena et al., 2016; Núñez et al., 2019). The boundary and initial conditions were defined analogously to the previous numerical experiments. Only the tide was considered, and the effect of the river was not included. Thus, the 15-daily tidal series shown in Fig. 8c—representative of the tide at the mouth of the Pas Estuary—was used. The initial conditions correspond to 10 min after the low tide of the neap tidal range. The parameters associated with the particle model are defined in Subsection 2.4.

### *4.3. Spatial evolution of the tide and its effect on the presence and accumulation of plastic debris*

Fig. 9a-b shows the $\gamma_1$ and $g_2$ of $d\eta/dt$ for the 15 days analysed in the Pas Estuary. The results are shown on maps and along two sections: A-A*—which corresponds to the main channel—and B-B*—which corresponds to the tidal flats—. $\gamma_1$ is close to zero—the characteristic value of symmetric tides—in the outer area near the estuary. However, the friction due to the sedimentary accumulation at the mouth transforms the external symmetric tide into a positive asymmetric tide at the mouth ($\gamma_1 = 0.2$). Tidal propagation through a channel whose section decreases in width and depth, i.e.,

© 2021. This manuscript version is made available under the CC-BY-NC-ND 4.0 license http://creativecommons.org/licenses/by-nc-nd/4.0/

friction increases, produces a positive trend in $\gamma_1$ that reaches a maximum value of 1.4 in the innermost area of the estuary (see $\gamma_1$ evolution in A-A* section). $\gamma_1$ also reaches values that exceed unity due to friction induced by shallow water over tidal flats; however, the intertidal storage that occurs near the boundaries of tidal flats reduces $\gamma_1$ (see $\gamma_1$ evolution in B-B* section). $g_2$, which ranges from -1.5 to 3, increases as the tide becomes more asymmetric and decreases in the opposite case. The increase in $\gamma_1$, which represents a greater difference between the intensities of flood/ebb currents, is due to a decrease in the duration of the flood phase and, therefore, is associated with a reduction in the frequency of the strongest flood currents, which is represented by the increase of $g_2$.

Fig. 9c shows the residual currents map associated with the above described $\gamma_1$ and $g_2$ and Fig. 9d shows the evolution of the residual currents along of the channel (A-A* section). From such figures, it is concluded that the most intense residual currents (0.1 m/s) are found in the ebb direction and occur in the proximity of the mouth. Between the mouth and up to approximately 3.3 km upstream, the ebb residual currents still predominate (0.05 m/s). However, the directions are reversed upstream of this area, where residual currents are in the flood direction and show a lower magnitude (0.007 m/s). The residual current pattern described by the astronomical tide within the Pas Estuary is analogous to that generated by the symmetric tide ($ATtype_{16}$) within the EC and ED geometries (see Fig. 5a).

Fig. 9d represents the residual currents of the Pas Estuary channel and the associated $\gamma_1 - g_2$ together with the pattern that relates $\gamma_1$, $g_2$, and residual currents from the numerical experiments. It is verified that the relationship between these parameters in the Pas Estuary conforms to the

© 2021. This manuscript version is made available under the CC-BY-NC-ND 4.0 license http://creativecommons.org/licenses/by-nc-nd/4.0/

inferred pattern of the experiments when a symmetric tide at the mouth drives hydrodynamics. The highest flood residual currents occur for $\gamma_1$ near 1 and $g_2$ near -0.25, while the lowest $\gamma_1$ and $g_2$ appear associated with the highest ebb residual currents.

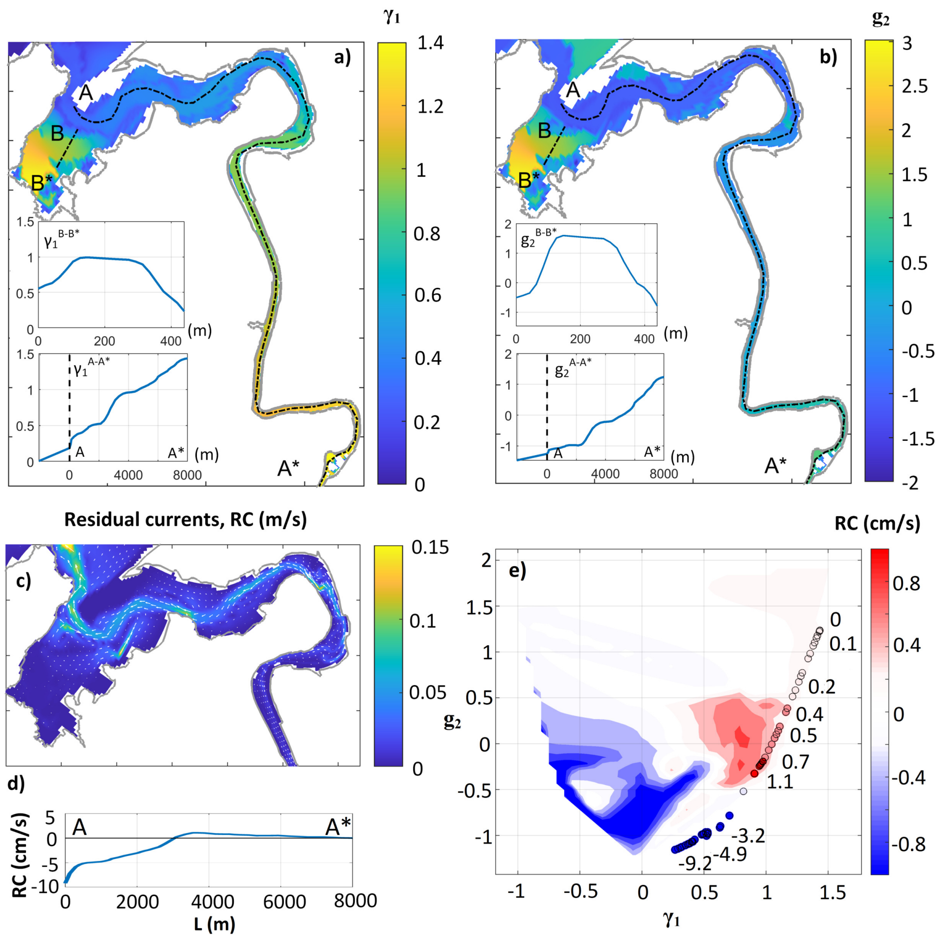


Figure 9: Tidal evolution through the Pas Estuary: a) Skewness ($\gamma_1$), b) Kurtosis ($g_2$), c) Residual currents (RC), d) RC along the channel (A-A* section), and e) relationship between RC$-\gamma_1 - g_2$ along A-A*.

© 2021. This manuscript version is made available under the CC-BY-NC-ND 4.0 license http://creativecommons.org/licenses/by-nc-nd/4.0/

Fig. 10a-b shows the average probability of the presence of particles ($P_m$) and the percentage of particles trapped on shoreline ($P_s$) at the end of the simulation. Fig. 10c aggregates these results along the estuary. Analogous behaviours are observed from the comparison of these aggregated $P_m$ and $P_s$ with those obtained by propagating $ATtype_{16}$ through the EC and ED geometries (see Fig. 7 and Tab. 1). An average presence of plastic debris is observed throughout the entire estuary, with $\sum P_m$ equal to 60%, which is similar to that of 70% obtained for the EC and ED geometries, and the highest concentrations in the innermost area. The presence of plastic debris becomes important upstream of 3.3 km from the mouth—due to the flood residual currents which are shown over this area—and in the curves that imply important changes in the flow direction, i.e., in areas close to 2.4, 3.3, and 4.2 km from the mouth (see Fig. 8c). The percentage of trapped particles within the Pas Estuary also follows a similar pattern than within the EC and ED geometries and shows a magnitude of the same order ($\sum P_s =$ 20%).

The average of $P_s$ in a 100 m radius and the average density of the plastic debris (AD) field data are compared in Fig. 10d. The non-parametric coefficient of Spearman (1961) ($\rho_s$) was applied to estimate the correlation between $P_s$ and $AD$ (Núñez et al., 2019). Sampling areas within the Pas Estuary which show higher AD, are close to areas where numerical modelling results in higher $P_s$, and vice versa. The $\rho_s$ coefficient between both series has a value of 0.78. The worst agreement occurs in the sampling areas located in the outer area of the estuary (sampling areas 7, 10, 11, and 12), where the waves and wind are likely influential as the tide was the only driver considered for analysis.

© 2021. This manuscript version is made available under the CC-BY-NC-ND 4.0 license http://creativecommons.org/licenses/by-nc-nd/4.0/

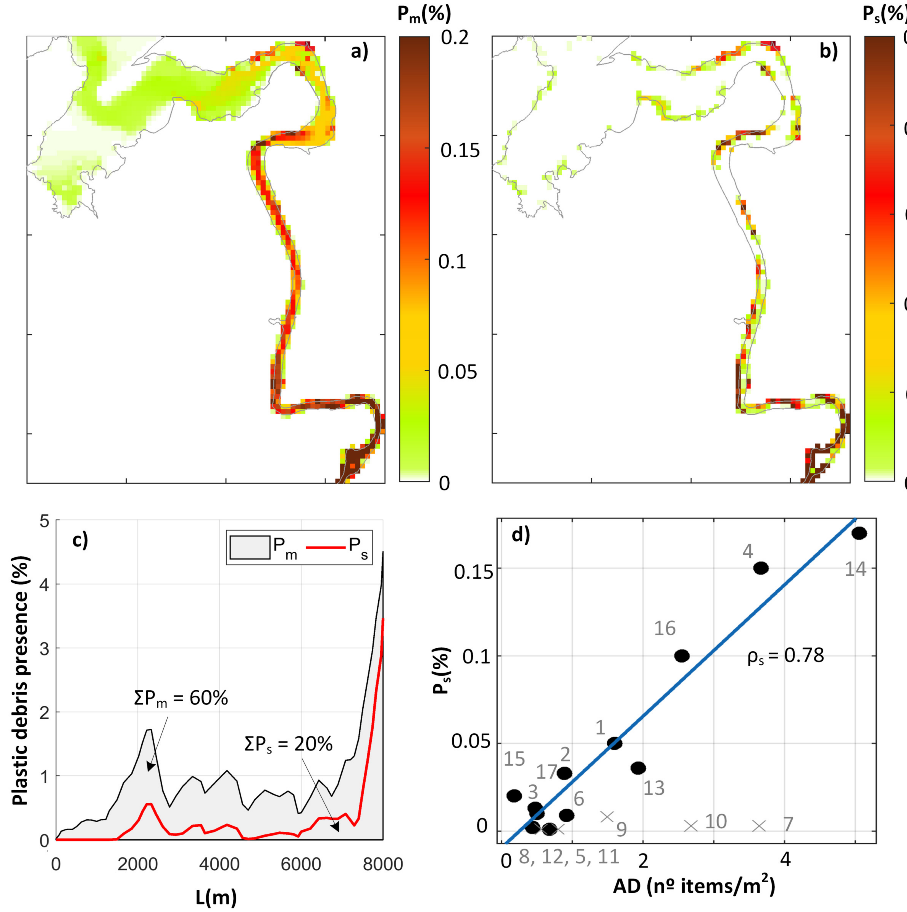


Figure 10: Tidal effect on plastic debris presence and accumulation within the Pas Estuary: a) Average probability of the presence of particles associated with a resolution of 50 m ($P_m/dx = 50$ m), b) percentage of particles trapped on the shoreline ($P_s/dx = 50$ m), c) accumulated $P_m$ and $P_s$ along the estuary, and d) comparison between $P_s$ and average density of plastic debris ($AD$).

© 2021. This manuscript version is made available under the CC-BY-NC-ND 4.0 license http://creativecommons.org/licenses/by-nc-nd/4.0/

## 5. Discussion

Tidal asymmetry at estuarine mouths as well as estuarine morphology are significant factors in determining flood or ebb dominance in tidal estuaries and, therefore, their ability to trap plastic debris.

Tidal asymmetry has traditionally been defined as the ratio between the amplitudes of two tidal constituents and the difference between both phases (Aubrey and Speer, 1985). However, other approaches should be used if tidal asymmetry arises from the interaction of a number of tidal constituents greater than two. Castanedo et al. (2007); Woodworth et al. (2005) proposed the use of the PDFs of the astronomical tide level. Nidzieko (2010); Song et al. (2011) recommended the use of the $\gamma_1$—a parameter related to the shape of the PDFs—of the tidal elevation time derivative ($d\eta/dt$) to represent the difference between the intensities of flood/ebb currents. The greater or lesser frequency of the strongest tidal currents in the asymmetry direction can be represented by the kurtosis coefficient Núñez et al. (2020). Consequently, the astronomical tide ability to transport plastic debris, or any other material into or out of tidal estuaries can be described in a complete way through the skewness ($\gamma_1$) and kurtosis ($g_2$) coefficients of $d\eta/dt$. The maximum transport ability toward the interior or exterior of the estuaries is achieved as a balance between the highest possible absolute value of $\gamma_1$, which indicates a greater difference between the flood and ebb current intensities, and the lowest values of $g_2$, which indicate higher frequencies of the strongest flood/ebb currents for positive/negative tidal asymmetry.

The evolution of $\gamma_1$ follows similar patterns for all analysed tides (symmetric and asymmetric) within the same estuarine geometry. In general, the $\gamma_1$ coefficient follows an increasing trend: positive asymmetry increases

© 2021. This manuscript version is made available under the CC-BY-NC-ND 4.0 license http://creativecommons.org/licenses/by-nc-nd/4.0/

and negative asymmetry decreases, with the bottom and lateral friction of the main channel. However, estuarine geometry is sometimes not associated with significant friction increases. In these cases, the tidal wave may not deform during its propagation, and consequently, $\gamma_1$ may remain unchanged or even experience a negative trend if it was initially. Furthermore, in estuaries that present sufficiently large tidal flat areas to counteract the deformation induced by the channel, any $\gamma_1$ may also be reduced. These conclusions on tidal deformation during propagation agree with the findings of Dronkers (1986), Friedrichs and Aubrey (1988), and Speer and Aubrey (1985), which only analysed the propagation of symmetric tides. For the evolutionary trend of $g_2$, it has been found that $g_2$ increases with the absolute value of $\gamma_1$, that is, when positive and negative asymmetry increase and decrease in the opposite case. Specifically, $g_2$ increases with the asymmetric nature of the tide, indicating that the frequency of the more intense flood/ebb currents decreases when tidal asymmetry becomes more positive/negative.

The evolution of $\gamma_1$ and $g_2$ arising from tidal propagations have some implications for the transport and dispersion of plastic debris within tidal estuaries. On the one hand, the tides whose asymmetry (positive or negative) increases as they propagate show increasing differences between the flood and ebb current intensities and, in principle, should show an increase in the transport capacity towards the estuary for positive asymmetry or towards the open ocean for negative asymmetry. However, because $g_2$ also increases with $|\gamma_1|$, the frequency of the most intense flood/ebb currents with positive/negative asymmetry decreases and partially offsets the increased transport intensity owing to $\gamma_1$. On the other hand, the tides whose asymmetry is reduced with propagation also show a reduction in $g_2$. Consequently, as long as some residual asymmetry remains, there will be a transport trend in

© 2021. This manuscript version is made available under the CC-BY-NC-ND 4.0 license http://creativecommons.org/licenses/by-nc-nd/4.0/

the direction of tidal dominance due to residual currents. From the obtained results, it was proven that the EC and ED geometries, which ideally represent common estuary configurations, always act as traps for plastic debris, confirming the findings of Acha et al. (2003) and Mazarrasa et al. (2019). Furthermore, the accumulation of plastic debris that has reached the mouth within estuaries is more likely if a positive asymmetry characterises the outer area.

To date, few previous studies have linked ocean tidal asymmetry and material transport, while all have focused on sediment transport (Moore et al., 2009; Nidzieko, 2010; Ranasinghe and Pattiaratchi, 2000). This study conducted a novel analysis of the transport of floating plastics representative of polypropylene, a material with a significant presence in the marine environment (Mazarrasa et al., 2019; Zhang, 2017), and incorporated the relative frequency of the strongest tidal currents through the kurtosis of $d\eta/dt$. Sediment transport in tidal channels is driven by settling/erosion asymmetry associated with tidal current asymmetry. However, the frequency of flood/ebb currents is also significant for evaluating plastic debris transport. This study demonstrated the importance of including kurtosis in the analyses because the $\gamma_1$-$g_2$ pair explains the complete distribution of tidal currents. The results indicate that the estuarine geometry conditions the probability patterns of plastic debris presence, that is, the location of the areas of high or low presence. However, the tidal type quantifies the magnitude of such a probability, which is higher for positive asymmetric tides and lower for both symmetric and negative asymmetric tides. This can be explained by the marine origin of plastic debris and tidal asymmetry imposed on estuarine mouths. If the tidal asymmetry in this area is positive, the greater intensity of the flood currents would favour a greater import of plastics that have

© 2021. This manuscript version is made available under the CC-BY-NC-ND 4.0 license http://creativecommons.org/licenses/by-nc-nd/4.0/

reached the mouth. Estuaries as important as the Dee estuary (on the west coast of the United Kingdom), Seine estuary (northern France), and Murray estuary (southern Australia), as well as the estuary where the Paraná and La Plata rivers flow (between Argentina and Uruguay), show positive asymmetric tides in the vicinity of their mouths, which conditions their import capabilities (Núñez et al., 2020). Conversely, if a tide is symmetric, its flood and ebb currents would be in equilibrium, and if it is negatively asymmetric, the ebb currents would be more intense. Consequently, the percentage of marine plastics that accumulate in estuaries subjected to symmetric or negative asymmetric tides at their mouths results from the evolution of ocean tidal asymmetry due to estuarine geometry and coastal trapping ability. Almost 89% of the world's coastal areas are symmetric (77.4%) and negative asymmetric tides (11.3%). The estuaries within these areas show a lower ability to import plastic debris. Estuaries such as Chesapeake Bay (on the east coast of the United States), San Francisco Bay (on the west coast of the United States), Thames Estuary (southeast coast of the UK), and Pas Estuary (northern coast of Spain) show symmetric tides at their mouths. The Severn Estuary (southwest coast of the UK), Swan River Estuary, Peel-Harvey Estuary, Wilson Inlet (on the southwest coast of Australia), Tomales Bay, Elkhorn Slough, and Tijuana River Estuary (in California), and Venice Lagoon (in the North Adriatic Sea) show external negative tidal asymmetry (Núñez et al., 2020).

It would be interesting for further research to analyse new representative estuarine geometries (e.g. larger bays), possible litter sources (e.g. river sources or uniform distributions of plastic debris), and the effects of plastic debris that reach estuaries in different tidal phases. Moreover, various factors in addition to tide may be influential and warrant further study, such

© 2021. This manuscript version is made available under the CC-BY-NC-ND 4.0 license http://creativecommons.org/licenses/by-nc-nd/4.0/

as river discharge, temperature, and salinity gradients, wind patterns, and waves (Browne et al., 2010; Carson et al., 2013; Zhang, 2017), the intrinsic properties of plastic debris such as specific density, size, and shape (Barnes et al., 2009; Kowalski et al., 2016; Chubarenko et al., 2016), and estuarine trapping ability (Mazarrasa et al., 2019; Viehman et al., 2011). The specific density, size, and shape of plastics influence buoyancy and therefore affect the transport and fate of plastic debris in marine environments. Depending on these features, plastic debris can be transported over the surface, in the water column, or through the bottom. To include this effect in the modelling, different values can be defined for the "specific density" and "settling velocity", which also depend on the size and shape of the particles (Isobe et al., 2014). Further laboratory studies are needed to acquire knowledge about these parameters and improve the quality of plastic debris modelling. Coastal trapping ability is decisive in the fate of plastic debris inside estuaries. This parameter shows spatial variability within each estuary and is strongly correlated with the presence and type of vegetation as well as with the flood-ebb regime. Studies such as those by Mazarrasa et al. (2019); Viehman et al. (2011) have detected high concentrations of plastic debris in the high marsh areas of estuaries that become especially significant in vegetated areas. This feature can be included within the modelling framework through the beaching parameter, one of the key parameters related to the modelling of the transport of any material. For substances such as hydrocarbons, there are specific studies that analyse the trapping ability of different types of shorelines and define these parameters for some oil spill models. In the case of plastic debris, there is insufficient knowledge about the interaction between different types of debris and different types of shorelines (Núñez et al., 2019). Overall, research on the transport and fate of plastic

© 2021. This manuscript version is made available under the CC-BY-NC-ND 4.0 license http://creativecommons.org/licenses/by-nc-nd/4.0/

debris within estuaries is still in its infancy, and there are many open fronts worth addressing in future research.

## 6. Conclusions

This research studies novel aspects of the effect of ocean tidal asymmetry and estuary morphology on tidal propagation and the fate of ocean plastic debris within tidal estuaries. Numerical experiments were performed by applying the hydrodynamic and Lagrangian transport models of Delft3D to four estuary types—corresponding to tidal creeks and defined by different cross-sectional areas that cause different frictions and tidal flat extensions—using three tidal types (selected according to their asymmetry) as boundary conditions. The parameters were selected to describe the tidal nature (i.e., skewness, which represents tidal asymmetry, and kurtosis, which refers to the frequency of the strongest tidal currents of the tidal elevation time derivative) and estuarine morphology (i.e., lateral boundary inclination, depth, and width of the main channel). In addition, this approach was applied to a real estuary, and a comparison with field data on plastic debris was performed. The results confirm previous findings regarding the evolution of symmetric tides and provide new considerations regarding the evolution of asymmetric tides and their effects on plastic debris distribution.

Symmetric tides evolve to positive asymmetric tides with propagation as the boundary and bottom friction of the channel increases; conversely, tidal asymmetry may experience a negative trend if the friction associated with lateral boundaries is weak or if the tidal flat area is large enough to counteract the effect of the channel. Symmetric tides explain the behaviour of estuaries located in 77.4% of the world's coastal areas; however, in the

© 2021. This manuscript version is made available under the CC-BY-NC-ND 4.0 license http://creativecommons.org/licenses/by-nc-nd/4.0/

remaining 22.6%, the tides show positive or negative asymmetry. As with symmetric tides, evolutionary trends of asymmetric tides are modulated by estuarine geometry, and the coefficient of skewness follows the same pattern; nevertheless, the value adopted by tidal skewness within estuaries is also conditioned by its external value. Analysing the propagation of asymmetric tides reveals that the initial skewness present at the mouths strongly conditions flood or ebb dominance and, therefore, the import of ocean plastic debris in estuarine areas where the main channel shows low flow opposition and favours tidal circulation. In this type of geometry, positive tidal asymmetry demonstrates an import capacity 50% higher than that of symmetric and negative asymmetric tides. In contrast, if there is a clear opposition to the flow or an important intertidal storage area, the relevant role in defining flood or ebb dominance is played by the geometry of the estuary, although small influences of the external tidal asymmetry are also appreciated. Thus, the probabilities of plastic debris presence are approximately 90% for positive asymmetric tides and 70-80% for symmetric or negative asymmetric tides.

The import and distribution of plastic debris within estuaries are not exclusively determined by the positive or negative skewness values—the kurtosis coefficient plays a notable role. The regulatory role of kurtosis, which corrects the tendency induced by skewness in the fate of plastics within tidal estuaries, is a key novel finding of this study. As the kurtosis increased, the asymmetric character of the tide increased as well. Thus, the frequency of the strongest flood currents is reduced for positive asymmetric tides and vice versa for negative asymmetric tides. Consequently, the astronomical tide's ability to transport plastic debris into or out of the estuary can be described comprehensively through the skewness and kurtosis coefficients.

© 2021. This manuscript version is made available under the CC-BY-NC-ND 4.0 license http://creativecommons.org/licenses/by-nc-nd/4.0/

## References

Abascal, A., Castanedo, S., Fernández, V., Medina, R., 2012. Backtracking drifting objects using surface currents from high-frequency (HF) radar technology. Ocean Dynamics 62, 1073–1089.

Abascal, A., Castanedo, S., Medina, R., Losada, I., Alvarez-Fanjul, E., 2009. Application of HF radar currents to oil spill modelling. Marine Pollution Bulletin 58, 238–248.

Abascal, A., Castanedo, S., Núñez, P., Mellor, A., Clements, A., Pérez, B., Cárdenas, M., Chiri, H., Medina, R., 2017. A high-resolution operational forecast system for oil spill response in Belfast Lough. Marine Pollution Bulletin 114, 302–314.

Abascal, A.J., Castanedo, S., Medina, R., Liste, M., 2010. Analysis of the reliability of a statistical oil spill response model. Marine Pollution Bulletin 60, 2099–2110.

Acha, E., Mianzan, H., Iribarne, O., Gagliardini, D., Lasta, C., Daleo, P., 2003. The role of the Río de la Plata bottom salinity front in accumulating debris. Marine Pollution Bulletin 46, 197–202.

Aubrey, D., Speer, P., 1985. A study of non-linear tidal propagation in shallow inlet/estuarine systems Part I: Observations. Estuarine, Coastal and Shelf Science 21, 185–205.

Balanda, K., MacGillivray, H., 1988. Kurtosis: a critical review. The American Statistician 42, 111–119.

Ballent, A., Purser, A., de Jesus Mendes, P., Pando, S., Thomsen, L., 2012.

© 2021. This manuscript version is made available under the CC-BY-NC-ND 4.0 license http://creativecommons.org/licenses/by-nc-nd/4.0/

Physical transport properties of marine microplastic pollution. Biogeosciences Discussions 9.

Barbier, E., Hacker, S., Kennedy, C., Koch, E., Stier, A., Silliman, B., 2011. The value of estuarine and coastal ecosystem services. Ecological monographs 81, 169–193.

Bárcena, J., García-Alba, J., García, A., Álvarez, C., 2016. Analysis of stratification patterns in river-influenced mesotidal and macrotidal estuaries using 3D hydrodynamic modelling and K-means clustering. Estuarine, Coastal and Shelf Science 181, 1–13.

Barker, C., Galt, J., 2000. Analysis of methods used in spill response planning: Trajectory Analysis Planner TAP II. Spill Science & Technology Bulletin 6, 145–152.

Barnes, D., Galgani, F., Thompson, R., Barlaz, M., 2009. Accumulation and fragmentation of plastic debris in global environments. Philosophical Transactions of the Royal Society B: Biological Sciences 364, 1985–1998.

Browne, M., Galloway, T., Thompson, R., 2010. Spatial patterns of plastic debris along estuarine shorelines. Environmental science & technology 44, 3404–3409.

Carmo, J.d., Pinho, J., Vieira, J., 2010. Oil spills in coastal zones: predicting slick transport and weathering processes. The Open Ocean Engineering Journal , 129–142.

Carson, H., Lamson, M., Nakashima, D., Toloumu, D., Hafner, J., Maximenko, N., McDermid, K., 2013. Tracking the sources and sinks of local marine debris in Hawaii. Marine environmental research 84, 76–83.

© 2021. This manuscript version is made available under the CC-BY-NC-ND 4.0 license http://creativecommons.org/licenses/by-nc-nd/4.0/

Castanedo, S., Mendez, F.J., Medina, R., Abascal, A., 2007. Long-term tidal level distribution using a wave-by-wave approach. Advances in Water Resources 30, 2271–2282.

Chubarenko, I., Bagaev, A., Zobkov, M., Esiukova, E., 2016. On some physical and dynamical properties of microplastic particles in marine environment. Marine Pollution Bulletin 108, 105–112.

Costa, M., Silva-Cavalcanti, J., Barbosa, C., Portugal, J., Barletta, M., 2011. Plastics buried in the inter-tidal plain of a tropical estuarine ecosystem. Journal of Coastal Research , 339–343.

Derraik, J., 2002. The pollution of the marine environment by plastic debris: a review. Marine Pollution Bulletin 44, 842–852.

Díaz, B., Pavón, A., Gómez-Gesteira, M., 2008. Use of a probabilistic particle tracking model to simulate the Prestige oil spill. Journal of Marine Systems 72, 159–166.

Dronkers, J., 1986. Tidal asymmetry and estuarine morphology. Netherlands Journal of Sea Research 20, 117–131.

Eerkes-Medrano, D., Thompson, R.C., Aldridge, D.C., 2015. Microplastics in freshwater systems: a review of the emerging threats, identification of knowledge gaps and prioritisation of research needs. Water research 75, 63–82.

Egbert, G., Erofeeva, S., 2002. Efficient inverse modeling of barotropic ocean tides. Journal of Atmospheric and Oceanic Technology 19, 183–204.

© 2021. This manuscript version is made available under the CC-BY-NC-ND 4.0 license http://creativecommons.org/licenses/by-nc-nd/4.0/

Feng, S., Cheng, R.T., Pangen, X., 1986. On tide-induced lagrangian residual current and residual transport: 1. lagrangian residual current. Water Resources Research 22, 1623–1634.

Friedrichs, C., Aubrey, D., 1988. Non-linear tidal distortion in shallow well-mixed estuaries: a synthesis. Estuarine, Coastal and Shelf Science 27, 521–545.

Galgani, F., Hanke, G., Maes, T., 2015. Global distribution, composition and abundance of marine litter, in: Marine anthropogenic litter. Springer, Cham, pp. 29–56.

Galgani, F., Hanke, G., Werner, S., De Vrees, L., 2013. Marine litter within the European marine strategy framework directive. ICES Journal of Marine Science 70, 1055–1064.

Galgani, F., Leaute, J., Moguedet, P., Souplet, A., Verin, Y., Carpentier, A., Goraguer, H., Latrouite, D., Andral, B., Cadiou, Y., et al., 2000. Litter on the sea floor along European coasts. Marine Pollution Bulletin 40, 516–527.

Gallo, F., Fossi, C., Weber, R., Santillo, D., Sousa, J., Ingram, I., Nadal, A., Romano, D., 2018. Marine litter plastics and microplastics and their toxic chemicals components: the need for urgent preventive measures. Environmental Sciences Europe 30, 13.

Galván, C., Juanes, J.A., Puente, A., 2010. Ecological classification of European transitional waters in the North-East Atlantic eco-region. Estuarine, coastal and shelf science 87, 442–450.

© 2021. This manuscript version is made available under the CC-BY-NC-ND 4.0 license http://creativecommons.org/licenses/by-nc-nd/4.0/

García, A., Sainz, A., Revilla, J.A., Álvarez, C., Juanes, J.A., Puente, A., 2008. Surface water resources assessment in scarcely gauged basins in the north of Spain. Journal of Hydrology 356, 312–326.

García Alba, J., García Gómez, A., Tinoco López, R.O., Sámano Celorio, M.L., García Gómez, A., Juanes de la Peña, J.A., et al., 2014. A 3-D model to analyze environmental effects of dredging operations-application to the Port of Marin, Spain .

Hall, K., 2000. Impacts of marine debris and oil: economic and social costs to coastal communities. Kommunenes Internasjonale Miljøorganisasjon.

Hinojosa, I., Thiel, M., 2009. Floating marine debris in fjords, gulfs and channels of southern Chile. Marine Pollution Bulletin 58, 341–350.

Hoitink, A., Hoekstra, P., Van Maren, D., 2003. Flow asymmetry associated with astronomical tides: Implications for the residual transport of sediment. Journal of Geophysical Research: Oceans 108.

Hydraulics, W.D., 2018a. Delft3d-FLOW Simulation of multi-dimensional hydrodynamic flows and transport phenomena, including sediments. User Manual, Delft-Holanda .

Hydraulics, W.D., 2018b. Delft3d-PART Simulation of mid-field water quality and oil spills, using particle tracking. User Manual, Delft-Holanda .

Iglesias, G., Carballo, R., 2010. Effects of high winds on the circulation of the using a mixed open boundary condition: the ría de Muros, Spain. Environmental Modelling & Software 25, 455–466.

Isobe, A., Kako, S., Chang, P.H., Matsuno, T., 2009. Two-way particle-tracking model for specifying sources of drifting objects: application to

© 2021. This manuscript version is made available under the CC-BY-NC-ND 4.0 license http://creativecommons.org/licenses/by-nc-nd/4.0/

the East China Sea Shelf. Journal of Atmospheric and Oceanic Technology 26, 1672–1682.

Isobe, A., Kubo, K., Tamura, Y., Nakashima, E., Fujii, N., 2014. Selective transport of microplastics and mesoplastics by drifting in coastal waters. Marine Pollution Bulletin 89, 324–330.

Jambeck, J., Geyer, R., Wilcox, C., Siegler, T., Perryman, M., Andrady, A., Narayan, R., Law, K., 2015. Plastic waste inputs from land into the ocean. Science 347, 768–771.

Jiménez, M., Castanedo, S., Zhou, Z., Coco, G., Medina, R., Rodriguez-Iturbe, I., 2014. Scaling properties of tidal networks. Water Resources Research 50, 4585–4602.

Kako, S., Isobe, A., Kataoka, T., Hinata, H., 2014. A decadal prediction of the quantity of plastic marine debris littered on beaches of the East Asian marginal seas. Marine Pollution Bulletin 81, 174–184.

Kako, S., Isobe, A., Magome, S., Hinata, H., Seino, S., Kojima, A., 2011. Establishment of numerical beach-litter hindcast/forecast models: An application to Goto Islands, Japan. Marine Pollution Bulletin 62, 293–302.

Klein, S., Worch, E., Knepper, T., 2015. Occurrence and spatial distribution of microplastics in river shore sediments of the Rhine-Main area in Germany. Environmental science & technology 49, 6070–6076.

Kowalski, N., Reichardt, A., Waniek, J., 2016. Sinking rates of microplastics and potential implications of their alteration by physical, biological, and chemical factors. Marine Pollution Bulletin 109, 310–319.

© 2021. This manuscript version is made available under the CC-BY-NC-ND 4.0 license http://creativecommons.org/licenses/by-nc-nd/4.0/

Kubota, M., 1994. A mechanism for the accumulation of floating marine debris north of Hawaii. Journal of Physical Oceanography 24, 1059–1064.

Law, K., Morét-Ferguson, S., Maximenko, N., Proskurowski, G., Peacock, E., Hafner, J., Reddy, C., 2010. Plastic accumulation in the North Atlantic subtropical gyre. Science 329, 1185–1188.

Lebreton, L.M., Greer, S., Borrero, J., 2012. Numerical modelling of floating debris in the world's oceans. Marine Pollution Bulletin 64, 653–661.

Lesser, G., Roelvink, J.v., Van Kester, J., Stelling, G., 2004. Development and validation of a three-dimensional morphological model. Coastal Engineering 51, 883–915.

Maximenko, N., Hafner, J., Niiler, P., 2012. Pathways of marine debris derived from trajectories of Lagrangian drifters. Marine Pollution Bulletin 65, 51–62.

Mazarrasa, I., Puente, A., Núñez, P., García, A., Abascal, A., Juanes, J., 2019. Assessing the risk of marine litter accumulation in estuarine habitats. Marine Pollution Bulletin 144, 117–128.

Moore, R., Wolf, J., Souza, A., Flint, S., 2009. Morphological evolution of the Dee Estuary, Eastern Irish Sea, UK: a tidal asymmetry approach. Geomorphology 103, 588–596.

Nidzieko, N., 2010. Tidal asymmetry in estuaries with mixed semidiurnal/diurnal tides. Journal of Geophysical Research: Oceans 115.

Núñez, P., Castanedo, S., Medina, R., 2020. A Global Classification of Astronomical Tide Asymmetry and Periodicity Using Statistical and Cluster Analysis. Journal of Geophysical Research: Oceans 125, e2020JC016143.

© 2021. This manuscript version is made available under the CC-BY-NC-ND 4.0 license http://creativecommons.org/licenses/by-nc-nd/4.0/

Núñez, P., García, A., Mazarrasa, I., Juanes, J.A., Abascal, A.J., Méndez, F., Castanedo, S., Medina, R., 2019. A methodology to assess the probability of marine litter accumulation in estuaries. Marine Pollution Bulletin 144, 309–324.

OSPAR, 2009. Marine litter in the North-East Atlantic Region: Assessment and priorities for response. London, United Kingdom , 127.

Ranasinghe, R., Pattiaratchi, C., 2000. Tidal inlet velocity asymmetry in diurnal regimes. Continental Shelf Research 20, 2347–2366.

Rech, S., Macaya-Caquilpán, V., Pantoja, J., Rivadeneira, M., Madariaga, D.J., Thiel, M., 2014. Rivers as a source of marine litter. A study from the SE Pacific. Marine Pollution Bulletin 82, 66–75.

Roelvink, J., Van Banning, G., 1995. Design and development of DELFT3D and application to coastal morphodynamics. Oceanographic Literature Review 11, 925.

Rubinstein, R.Y., Kroese, D.P., 1981. Simulation and the Monte Carlo method. volume 10. John Wiley & Sons.

Song, D., Wang, X., Kiss, A., Bao, X., 2011. The contribution to tidal asymmetry by different combinations of tidal constituents. Journal of Geophysical Research: Oceans 116.

Spearman, C., 1961. The proof and measurement of association between two things. .

Speer, P., Aubrey, D., 1985. A study of non-linear tidal propagation in shallow inlet/estuarine systems Part II: Theory. Estuarine, Coastal and Shelf Science 21, 207–224.

© 2021. This manuscript version is made available under the CC-BY-NC-ND 4.0 license http://creativecommons.org/licenses/by-nc-nd/4.0/

UNEP, 2005. Marine Litter: An Analytical Overview. UNEP.

van Utenhove, E., 2019. Modelling the transport and fate of buoyant macroplastics in coastal waters. Ph.D. thesis. Delft University of Technology.

Van Sebille, E., England, M., Froyland, G., 2012. Origin, dynamics and evolution of ocean garbage patches from observed surface drifters. Environmental Research Letters 7, 044040.

Viehman, S., Vander P, J.L., Schellinger, J., 2011. Characterization of marine debris in North Carolina salt marshes. Marine Pollution Bulletin 62, 2771–2779.

Viikmäe, B., Torsvik, T., Soomere, T., 2013. Impact of horizontal eddy diffusivity on Lagrangian statistics for coastal pollution from a major marine fairway. Ocean Dynamics 63, 589–597.

Westfall, P., 2014. Kurtosis as peakedness, 1905–2014. rip. The American Statistician 68, 191–195.

Woodworth, P., Blackman, D., Pugh, D., Vassie, J., 2005. On the role of diurnal tides in contributing to asymmetries in tidal probability distribution functions in areas of predominantly semi-diurnal tide. Estuarine, Coastal and Shelf Science 64, 235–240.

Yonkos, L., Friedel, E., Perez-Reyes, A., Ghosal, S., Arthur, C., 2014. Microplastics in four estuarine rivers in the Chesapeake Bay, USA. Environmental science & technology 48, 14195–14202.

Yoon, J.H., Kawano, S., Igawa, S., 2010. Modeling of marine litter drift and beaching in the Japan Sea. Marine Pollution Bulletin 60, 448–463.

© 2021. This manuscript version is made available under the CC-BY-NC-ND 4.0 license http://creativecommons.org/licenses/by-nc-nd/4.0/

Zambianchi, E., Iermano, I., Suaria, G., Aliani, S., 2014. Marine litter in the Mediterranean Sea: an oceanographic perspective, in: CIESM Workshop Monograph 46: Marine litter in the Mediterranean and Black Seas, CIESM Publisher Monaco. pp. 31–41.

Zambianchi, E., Trani, M., Falco, P., 2017. Lagrangian transport of marine litter in the Mediterranean Sea. Frontiers in Environmental Science 5, 5.

Zhang, H., 2017. Transport of microplastics in coastal seas. Estuarine, Coastal and Shelf Science 199, 74–86.

Zhou, Z., Olabarrieta, M., Stefanon, L., D'Alpaos, A., Carniello, L., Coco, G., 2014. A comparative study of physical and numerical modeling of tidal network ontogeny. Journal of Geophysical Research: Earth Surface 119, 892–912.